Energy performance analysis of a novel solar PVT loop heat pipe employing a microchannel heat pipe evaporator and a PCM triple heat exchanger

Thierno M.O. Diallo[a, *]

~~tdiallo.hull@gmail.com~~thierno.diallo@cstb.fr

Min Yu[a]

Jinzhi Zhou[a]

Xudong Zhao[a]

Samson Shittu[a]

Guiqiang Li[a]

Jie Ji[b]

David Hardy[a]

[a]School of Engineering, University of Hull, United Kingdom

[b]University of Science and Technology of China, Heifei, China

[*]Corresponding author.

Abstract

This study presents a numerical analysis of the energy efficiency for a novel solar PVT Loop Heat Pipe (PVT-LHP) employing a novel Micro-channel evaporator and a novel PCM heat storage exchanger. It presents a description of the different sub-models in the PVT-LHP system (the PVT model, the microchannel heat collector model and the novel PCM triple heat exchanger model) and the integrated model of the system. The integrated model of the system was solved by ensuring a heat balance at the condenser and the evaporator. A parametric analysis has been performed in order to assess the influence of the environmental parameters (i.e. solar radiation, air temperature, wind velocity), structural parameters (i.e. glazing cover, the number of absorbing microchannel heat pipes, PV cell packing factor), the circulating fluid variables (i.e. cold-water inlet temperature and water mass flow rate) on the energy performance of the system. The novel PVT-LHP has been compared with a conventional Solar PVT-LHP system. It was found that lower solar radiation, lower ambient air temperature, higher wind speed, higher packing factor, lower cold-water inlet temperature and a smaller cover number led to an enhanced electrical efficiency, but a reduced thermal efficiency of the module; whereas a higher cold-water mass flow rate and a greater number of microchannel heat pipes gave rise to both thermal and electrical efficiencies of the module. It was also found that an increase of solar radiation, ambient temperature, cover number, microchannel heat pipe number and packing factor are favourable factors for the overall COP (Coefficient Of Performance) of the system, whereas an increase of wind velocity and cold water mass flow rate are unfavourable. The study indicated the existence of an optimal cover number, number of microchannel heat pipes and mass flowrate. Under the given design conditions, the electrical, thermal and overall efficiency of the PV/LHP module were 12.2%, 55.6% and 67.8% respectively and the novel system can achieve 28% higher overall energy efficiency and 2.2 times higher COP compared to a conventional system. The integrated computer model developed in this study can be used to design and optimize the novel PVT-LHP heating system.

Keywords: PVT; Loop heat pipe; Microchannel; PCM triple heat exchanger; Heating; Power supply

Nomenclature

A

area [m^2]

a

mini-channel width [m]

b

mini-channel height [m]

Bo

Bond number [m]

C

heat capacity [W/K]

C, d

discharge coefficient [−]

D, d

diameter [m]

e

thickness [m]

f

liquid fraction, friction factor [−]

g

gravitational acceleration 9.81 [m/s^2]

G

mass velocity [kg/m^2/s]

H

height [m]

h

heat transfer coefficient [W/m^2/K]

h_{fg}

latent heat of vaporisation [J/kg/K]

k

thermal conductivity [W/m/K]

L

length [m]

m

variable [m^{-1}]

N

number [−]

N_{ch}

number channel ports [−]

Nu

Nusselt number [−]

P

pressure [Pa]

ΔP

pressure drop [Pa]

q

heat density [W/m^2]

Q

heat transfer rate [W]

Ro

specific gas constant [J/(kg K)]

R

radius [m]

R

thermal resistance [W/K]

Re

Reynolds number [−]

t/T

temperature [ºC/ºK

U

heat loss [W/K]

u

velocity [m/s]

W

collector width [m]

x

vapour quality [−]

Subscripts

an

annular

av

average

c

cold, charge, cover

ch

channel

cond

condensation

d

discharge

f

fin

F

efficiency factor

e

evaporator, electrical

eq

equivalent

ei

electrical insulation

EVA

ethylene-vinyl acetate

fg

fluid gas

g

gravity

i

inlet

min

minimum

mt

middle tube

h

hole, header

he

heat exchanger

hp

heat pipe

hp-he

heat pipe to heat exchanger

lf

the liquid film

lh

liquid header

LO

liquid only

ltl

liquid transportation line

vtl

vapour transportation line

l

liquid

L

loss

lf

liquid film

o

overall

out

outlet

p

PV cell

PCM

phase change material

Pr

Pranlt

p-fin

PV-Fin

th

thermal

tp

two-phase

u

utile

v

vapour

vtl

vapour transportation line

w

water

Greek symbols

β

packing factor [-]

ε

efficiency [-]

Δ

difference

λ

thermal conductivity [W/(m K)]

μ

dynamic viscosity [Pa.s]

ρ

density [kg/m^3]

δ

thickness [m]

η

efficiency [m]

σ

surface tension [N/m]

v

specific volume [m^3/kg

1 Introduction

The increasing frequency of extreme weather events observed around the world in recent years is confirming, more than ever, the reality of climate change, as such it is increasingly urgent to intervene in order to decrease global carbon emissions. For this purpose, it is necessary to develop efficient and low cost renewable technologies to decrease fossil fuel reliance and consequently carbon emissions. Today, PV technologies represent one of the measures that can increase the renewable energies share. They represent a great potential to deliver around 5% of global electricity demand by 2030 and 11% by 2050 [1]. In the last decade several studies have been performed on the research and development of PVT systems [2–4] because they can offer higher power output than a standard PV, and they can be cost effective if the thermal component is cheap [5]. It is recognized that PVT technology has the advantage to cool PV cells and then increase their electrical output [6]. However, the market of PVT systems is still very low compared to PV and thermal markets. In fact, in cold climates the PVT systems are not able to meet all hot water and space heating yearly demands [7]. In order to increase their market share, there is a need to develop highly efficient, lower cost and reliable systems. One of the technologies developed to enhance the efficiency of PVT systems is PVT-LHPs. The use of LHPs in PVT systems can enhance the heat transfer at the heat pipe's evaporator and transfer a large amount of heat over a long distance. By definition, Loop Heat Pipes (LHPs) are two-phase heat transfer (evaporation/condensation) devices that are able to transfer large amount of heat over long distances because of a capillary or gravitational structure [8,9]. The major advantages of LHPs, compared to Heat Pipes (HPs), is the ability to operate against gravity and achieve a higher maximum heat transport capacity [8]. Due to these main advantages, LHPs are ideally suitable for use in solar collection systems for hot water and space heating. Today, existing solar PVT-LHPs are not technically mature [10]; there are still opportunities to enhance their thermal performance [3]. An efficient way to enhance the thermal performance of Solar PVT-LHPs could be to enhance the heat transfer at

the evaporator by using Mini-Channel Heat Pipes (MCHPs), a method which has not yet been investigated and reported. However, the use of mini-channels in standard heat pipe collectors have been numerically and experimentally investigated [11–16]. The increase in heat collection at the evaporator can be beneficial for PVT panel, as more heat collection means a reduced PV cell temperature (the PV cells are cooled) and higher power output [3]. The flow pattern in the microchannel heat pipe can also impact the PVT performance, Valeh-e-Sheyda et al. [17] performed a study of two-phase flow (air and water) in a small hybrid micro-channel solar cell consisting on an array of rectangular microchannels with a hydraulic diameter of 0.667 mm. They showed that the type of flow pattern in a microchannel can significantly impact the efficiency of the hybrid PV system. They found that the two-phase slug flow pattern gives higher PV performance compared with a single-phase flow. Alternatively, another way to increase the thermal efficiency of PVT-LHPs is to enhance the efficiency of the condenser by increasing the condensation heat transfer and the increase of the total heat transferred to the water. As the solar radiation is intermittent, a way to increase this total heat transfer rate could be the use of energy storage in the heat exchanger. A PCM heat exchanger can help to store the excess heat and release it when there is an energy demand, during the night or the day, due to lower solar radiation. This way to improve the thermal performance of solar LHPs has also not been investigated or reported.

In this paper, a novel PVT-LHP has been proposed, utilising a micro-channel heat pipe at the evaporator and PCM heat storage at the condenser. First, the paper describes the new PVT-LHP, then it presents the numerical model developed to assess the behaviour of the system and its energy efficiency. A parametric study has been performed to assess the influence of the key environmental and structure parameters on the energy efficiency of the system. Finally, the efficiency of the system has been compared with a conventional PVT-LHP. The theoretical model developed in this paper will help to design and optimize such system for space heating, hot water and power supply.

2 Presentation of the novel solar PVT- LHP system

The PVT-LHP system is described in Fig. 1. The loop is filled with the refrigerant R-134a. Water is not used as refrigerant because it is chemically incompatible with the aluminium microchannel. In fact, the interaction of water with aluminium can lead to a corrosive reaction without natural inhibition. This corrosion can generate non-condensable gas which causes the internal vacuum to break, resulting in failure of the heat pipe [18]. The PVT-LHP system is composed of the following main elements: the outside cover, the PV cells, the aluminium absorber, the evaporator microchannel heat pipe, the condensate liquid return pathway (Fig. 2 a, b, c), the triple PCM heat exchanger, the vapour transportation line, the liquid transportation line, the liquid header, and the liquid collector at the bottom of the evaporator. The evaporated fluid in the mini-channel is collected at the vapour header and transferred towards the PCM heat exchanger through the vapour transportation line. The PCM heat exchanger (Fig. 2 d, e) is composed of three tubes: the central tube containing the refrigerant, the middle tube containing the water and the outer tube containing an organic PCM material. At the condenser, the heat from the evaporated fluid arriving in the central tube is transferred to the water in the middle tube. Then the heated water in the middle channel causes the fusion/melting of the PCM at the outer channel tube to store the excess heat. The PCM material is placed in the outer tube of the heat exchanger rather than in the middle tube to avoid any blockage of the heat transfer from the refrigerant to the water due to the PCM's potential to freeze. After condensation in the central tube of the heat exchanger, the liquid returns to the refrigerant header and enters to the evaporator through small holes (Figs. 1 and 2 b). The natural fluid circulation in the LHP system is governed by the pressure head between the condenser and the bottom of the evaporator. The PVT collector is composed of 20 Mini-channel Heat Pipes. Each mini-channel is composed of 10 ports (Fig. 2 c). The condensed liquid enters into each port via four small holes with 0.75 mm diameter. The holes are placed on one side of each mini-channel port (Fig. 2c). They do not exist at the opposite side of the wall to avoid blocking the vapour flow when the evaporator is inclined, because of a different gravitational effect. The adiabatic part of the PVT is composed of two insulated transportation lines (the insulation of the two transportation lines and the heat exchanger are shown in Fig. 1).

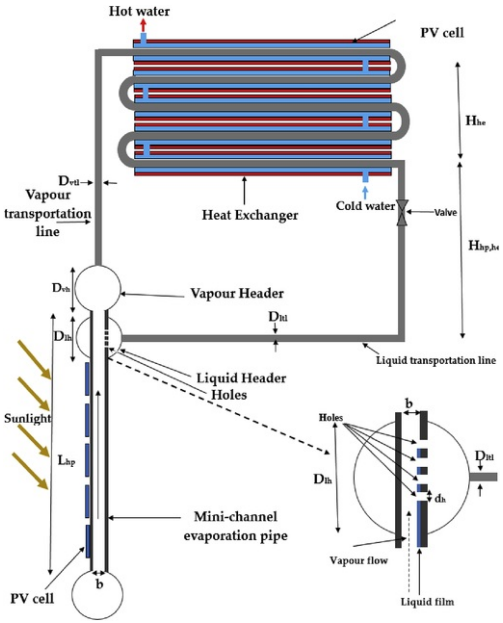

Fig. 1 Schematic of the novel Solar Loop Heat Pipe.

alt-text: Fig. 1

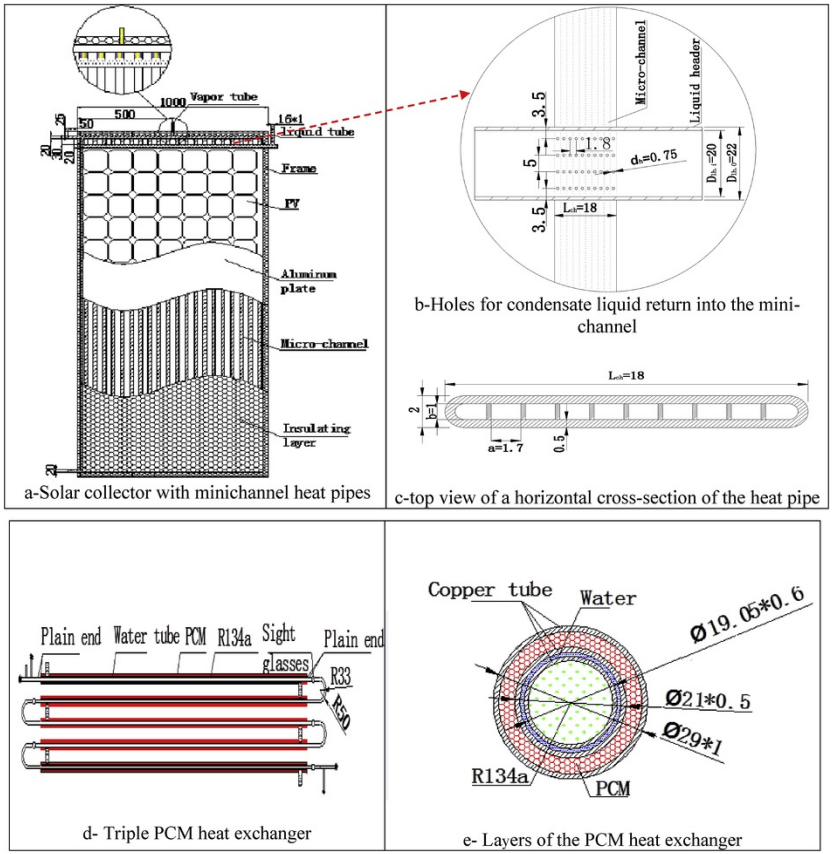

Fig. 2 Solar collector with minichannel heat pipes, condensate liquid pathway and the PCM heat exchanger (units in mm).

alt-text: Fig. 2

Table 1 summarises the designed parameters of the LHP system components (these values will be used to study experimentally the thermal performance of the system). The physical characteristics of the glazing cover, PV Cell, EVA and electrical insulation are presented in Annex 1.

Table 1 Design parameters of the LHP operation and heat exchanger.

alt-text: Table 1

Parameters	Nomenclature	Value	Unit
Mini-channel port width	a	0.0017	m
Mini-channel port height	b	0.001	m
Evaporator length	L_{hp}	1.9	m
Number of mini-channel heat pipes	N_{hp}	20	–
Number of mini-channel ports	N_p	10	–
Total number of mini-channel ports	N_{ch}	200	–

Operating temperature range	t_v	20–60	°C
Evaporator to condenser height difference	$H_{hp\text{-}he}$	0.6	m
Transportation line outer diameter	$D_{ltl,o}/D_{vtl,o}$	0.015	m
Transportation line inner diameter	$D_{ltl,i}/D_{vtl,i}$	0.0174	m
Liquid head length	L_{lh}	1	m
Liquid Head diameter	D_{lh}	0.022	m
Vapour header length	L_{vh}	1	m
Hole diameter	d_h	0.00075	m
Transportation line length	L_{ltl}/L_{vtl}	1/1	m
Heat exchanger central tube total length	L_{he}	5	m
Heat exchanger central tube diameters	D_1/D_2	0.016/0.017	m
Heat exchanger middle tube diameters	D_2/D_4	0.019/0.021	m
PCM tube diameters	D_5/D_6	0.027/0.029	m
PCM melting temperature	T_{pcm}	44	°C
PCM density	ρ_{pcm}	800	kg/m^3
PCM Latent Heat	L_h	242	kJ/kg
PCM thermal conductivity	λ_{pcm}	0.18	W/mK
PCM Maximum operating temperature	$T_{pcm\text{-}max}$	300	°C

3 Mathematical model of the solar energy conversion

This section presents the theoretical models developed in order to analyse the behaviour of the system and to assess its energy performance. Fig. 3 presents the heat transfer process from ambient air to the micro-channel heat pipe evaporator. This heat transfer includes four processes (as shown in Fig. 3):

1) Absorption of part of the solar radiation and dissipation of the remaining heat into the ambient air.

2) Conversion of part of the absorbed energy into electricity through PV cells.

3) Transportation of the remaining part of the absorbed energy into the passing refrigerant in the microchannel heat pipe. The evaporated refrigerant flows towards the PCM heat exchanger.

4) Transfer of the heat from the central tube of the Triple PCM heat exchanger to the middle tube containing the water.

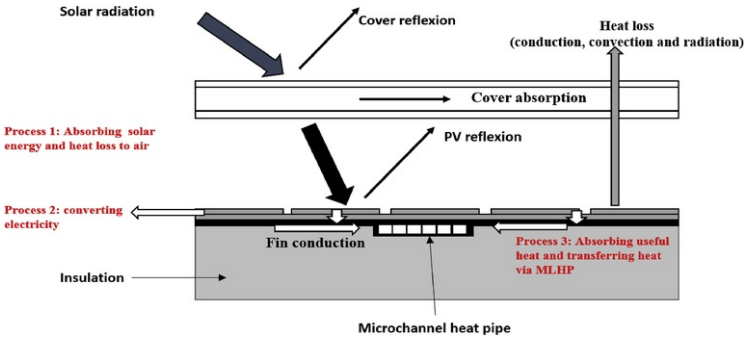

Fig. 3 Heat transfer from ambient air to the microchannel evaporator.

alt-text: Fig. 3

3.1 Model of the heat transfer from the ambient air to the microchannel evaporator

Fig. 3 presents the heat transfer process from the outside air to the microchannel evaporator. The heat transfer model from the surrounding air to absorber plate is presented in Annex 2 [19].

This LHP involves a number of thermal resistances that result in changing the working fluid temperature, which is detailed as follows (Fig. 4). The resistance of the silicon sealant is ignored because of its significantly smaller value compared to the other factors.

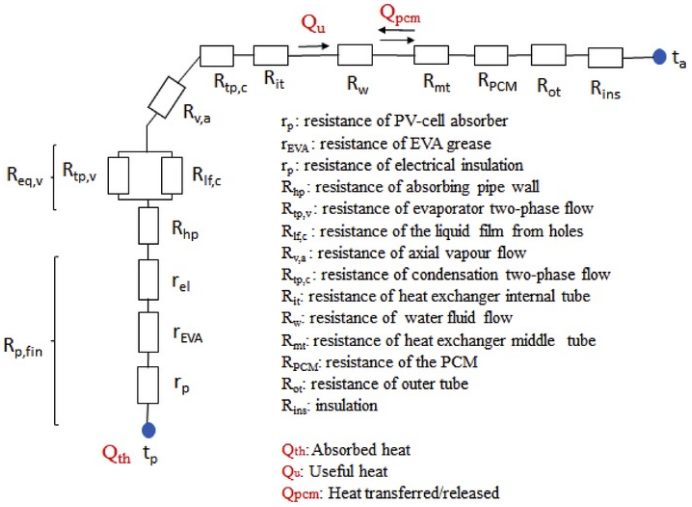

Fig. 4 Schematic of heat transfer along the PVT-LHP.

alt-text: Fig. 4

The total useful solar heat received by the water in the middle tube of the PCM triple heat exchanger is expressed through the Hottel-Whillier model [19,20] from fin to microchannel:

$$Q_u = L\,W\,F_{th}\left[q_{abs} - U_L\left(T_{c,av} - T_a\right) - q_e\right] \quad \textbf{(1)}$$

where, L and W are respectively the length (m) and width (m) of the fin sheet; q_{abs} is the absorbed heat (related to the solar radiation), UL (W/K) is the heat loss (and integrate the impact of the wind velocity, see Annex 2); q_e is the energy converted to electricity, $T_{c,av}$ is the mean temperature of water at the central tube of the PCM heat exchanger, T_a is the ambient temperature; F_{th} is the collector thermal efficiency factor, defined as following:

$$F_{th} = \frac{\frac{1}{U_L}}{\frac{LW}{N_{hp}}\left\{\frac{1}{LU_L\left[\left(\frac{W}{N_{hp}}-L_{hp}\right)F_f+\frac{L_{hp}}{1+r_{p-fin}U_L}\right]}+\sum_{i=1}^{6}R_i\right\}} \quad (2)$$

This efficiency factor considers all the thermal resistances from the fin to the water in the middle tube of the PCM triple heat exchanger: (1) thermal resistances between the PV cells and heat pipe fins $R_{p\text{-}fin}$; (2) thermal resistance of the heat pipe R_{hp}; (3) equivalent radial thermal resistance of the of flow $R_{eq,v}$, this resistance is composed of the resistance of the liquid film from the holes on one side of the channel $R_{lf,c}$ that is assumed parallel to the radial thermal resistance of the two phase flow on the other sides of the channel $R_{eq,v}$; (4) the resistance of axial vapour flow $R_{v,a}$; (5) the resistance of the condensation two phase flow $R_{tp,c}$; (6) the thermal resistance of the PCM heat exchanger central tube R_{it}.

Thermal resistances between the PV cells and heat pipe fins $R_{p,fin}$, Heat transfer between the PV module and heat pipe fins is a conventional one-dimensional multi-layer heat conduction process and its associated thermal resistance is [19]:

$$R_{p-fin} = r_p + r_{EVA} + r_{ei} = \frac{\delta_p}{k_p} + \frac{\delta_{EVA}}{k_{EVA}} + \frac{\delta_{ei}}{k_{ei}} \quad (3)$$

Where, $r_{p\text{-}fin}$, r_p, r_{EVA} and r_{ei} are respectively the thermal resistances per unit area (m^2-K/W) of PV cells to fin sheet, PV cells, EVA layer and electrical insulation; kp, k_{EVA}, k_{ei}, δ_p, δ_{EVA}, and δ_{ei} are respectively the thermal conductivity (W/m/K) and thickness (m) of PV layer, EVA layer and electrical insulation. Where, N_{hp} is the number of heat pipes; $\sum Ri$ is the overall thermal resistance from the fin sheet to the refrigerant (W/m/K). The standard fin efficiency, F_f, is defined as:

$$F_f = \frac{\tanh\left[m\left(W/N_{hp}-L_{hp}\right)/2\right]}{m\left(W/N_{hp}-L_{hp}\right)/2} \quad (4)$$

Where the variable m, is given by:

$$m = \sqrt{\frac{U_L}{k_f\delta_f\left(1+r_{p-fin}U_L\right)}} \quad (5)$$

Thermal resistance of heat pipe wall, R_{hp}, Heat transfer through the heat pipe wall is a typical steady-state conduction process, and its thermal resistance can be written as:

$$R_{hp} = \frac{e_{hp}}{k_{hp}\ \left(2\times(a+b)\times L_{hp}\right)\ N_{hp}} \quad (6)$$

Thermal resistance of evaporation, $R_{v,eq}$: the thermal resistance of the condensate liquid film from the holes flowing along the heat pipe wall is assumed to be parallel to thermal convective two phase resistance of the three other sides of the channel port. The equivalent thermal resistance is expressed as follows:

$$R_{eq,v} = \left(\frac{1}{R_{tp,v}}+\frac{1}{R_{lf,v}}\right)^{-1} \quad (7)$$

The total resistance of the condensate liquid film $R_{lf,v}$ of thickness δ_{lf} at the adjacent sides of the micro channel holes is expressed as follows:

$$R_{lf,v} = \frac{\delta_{lf}}{k_w\left(a\times L_{hp}\right)\ N_{hp}\ N_{ch}} \quad (8)$$

The resistance of the two-phase flow is expressed as follows:

$$R_{tp,v} = \frac{1}{(a+2b)\quad \varepsilon_{of}\ \ L_{hp}\ \ h_{tp}\ N_{hp}} \quad (9)$$

The two-phase overall heat transfer coefficient h_{tp} in the microchannel is expressed by considering the overall efficiency of fins ε_{of} in the microchannel heat pipe. The expression of ε_f and h_{tp} are presented in the Annex 3. The liquid film thickness δ_{lf} is linked to the pressure difference between the top of the evaporator and the outlet of the condenser H_{ce} (Fig. 1). This liquid film is formed by the condensate liquid from the four holes of the mini-channel

(Fig. 1). The thickness of the liquid film with a current flow may be approximated to that without one, because the film thickness with counter current flow becomes a little larger that without it [21]. The liquid film thickness δ_{lf} can be approximated as follows:

$$\delta_{lf} = \left(\frac{3\mu_l^2}{\rho_l^2 g}\right)^{1/3} Re^{1/3} \text{ for } Re \leq 400 \quad (10)$$

And

$$\delta_{lf} = 0.369\left(\frac{3\mu_l^2}{\rho_l^2 g}\right)^{1/2} Re^{1/2} \text{ for } Re>400 \quad (11)$$

With: *Re* the Reynolds number, μ_l (Pa.s) the liquid dynamic viscosity, g (m/s^2). The Reynolds number is given by:

$$Re = \frac{\rho_l U_l \delta_{lf}}{\mu_l} \quad (12)$$

U_l is the superficial velocity of the liquid film. As the liquid flow through the small holes of the microchannel depends of the driving force of the loop, which is the pressure head, it is suitable to correlate it with the superficial flow. Then, the superficial velocity u_l is linked to the pressure head by the following equation (it is simply expressed as a liquid flowing throughout a hole because of the pressure head):

$$u_l = A_h \frac{\left(2g\, H_{hp-he}\right)^{\frac{1}{2}}}{A_l\ \left(1 - Cd^2\left(d_h/D_{lh}\right)\right)} \quad (13)$$

Where A_h is the hole's section, $H_{hp\ -\ he}$ is the pressure head (height difference between the top of the evaporator and the heat exchanger), d_h is the hole's diameter, D_{lh} is the diameter of liquid header. The mass velocity u_l is assumed the same for the four holes, then the film thickness is assumed the same along the adjacent wall. A_l is the liquid film section expressed as follows:

$$S_l = \delta_{lf}\, a \quad (14)$$

a is the mini-channel port width. Cd [−] is, the discharge coefficient of the flow from the liquid head to the hole and expressed as follows [22]:

$$C_d = 0.611\left[87\left(\frac{\mu_l}{\rho_l\, d_h \sqrt{g\, H_{hp,he}}}\right)^{1.43} + \left(1 + \frac{4.5\ \mu_l}{\rho_l\, d_h \sqrt{g\, H_{hp,he}}}\right)^{-1.26}\right]^{-0.7} \quad (15)$$

The liquid thickness δ_{lf} is calculated iteratively by assuming that the liquid mass flow from the liquid header is equal to the mass flow of the liquid film.

Thermal resistance of axial vapour flow, $R_{v,a}$, The vapour flow process from the evaporation section to the condensing heat exchanger experiences a certain pressure loss and consequently a temperature drop. This creates a resistance in heat transfer which could be written as:

$$R_{v,a} = \frac{T_v^2 R_0 \Delta P_v\ N_{hp}\ N_{ch}}{Q_u\ h_{fg} P_v} \quad (16)$$

The total pressure drop of the system has been expressed as given in Ref. [23].

Thermal resistance of the condensation, R_{cond}, Heat transfer through the heat pipe wall is a typical steady-state conduction process, and its thermal resistance can be written as:

$$R_{cond} = \frac{1}{2 \uparrow \pi d_l L_{hx} h_{cond}} \quad (17)$$

The condensation heat transfer coefficient h_{cond} is given in Annex 3.

3.2 Mathematical model of the heat transfers in the heat triple heat exchanger

In the heat pipe's evaporation section, part of the solar energy converted into heat Q_u, leads to the evaporation of the heat pipe working fluid. This vapour fluid moves forward to the condensing triple heat exchanger, via the vapour transportation line, where the evaporated fluid is condensed and transfers the condensation heat into the adjacent water flow and surrounding PCM. The condensed fluid in the central tube of the heat exchanger returns to the

evaporation section, via the liquid transportation line, thus forming a complete heat transportation cycle. Fig. 5 presents the heat exchanger geometry.

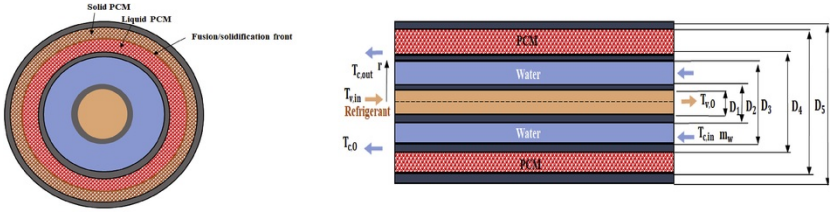

Fig. 5 Sketch map of phase change process.

alt-text: Fig. 5

There are two heat transfer process in the water middle tube according to the charge or discharge of the PCM. The NTU (Number of Transfer Units) method is used to quantify the heat transfer rate from the water to the PCM material.

3.2.1 Charging the PCM

The heat transferred from water in the middle tube to the PCM is expressed as following:

$$Q_c = \varepsilon_c C_{min} \left(T_{c,out} - T_{c,in}\right) \quad \textbf{(18)}$$

With C_{min} (W/K) is the minimum heat transfer capacity, ε_c is the average effectiveness of the melting process and is expressed as follows [24]:

$$\varepsilon_c = \int_0^1 (1 - \exp(-\frac{1}{R_T C_{min}})) \, df \quad \textbf{(19)}$$

Where f is the fraction of melted PCM and varies from 0 (only solid) to 1 (only liquid), R_T is the total resistance from the water to the PCM material and is expressed as follows:

$$R_T = R_w + R_{mt} + R_{PCM} \quad \textbf{(20)}$$

Where R_w is the water resistance, R_{mt} is the resistance of the middle tube and R_{PCM} is the resistance of the PCM. The different resistances are expressed as follows:

$$R_w = \frac{1}{h_w \pi D_2 L_{he}} \quad \textbf{(21)}$$

The convective heat transfer coefficient h_w of the water on the annulus side can be calculated by

$$h_w = \frac{Nu \, k_w}{D_{45}} \quad \textbf{(22)}$$

The Nusselt number *Nu* of the annulus water flow is given in Annex 4:

Thermal resistance of the middle tube R_{mt}, the conductive thermal resistance of the middle tube is expressed as follows:

$$R_{mt} = \frac{1}{2 \pi k_{mt} L_{he}} \log\left(\frac{D_4}{D_3}\right) \quad \textbf{(23)}$$

Thermal resistance of the PCM R_{PCM}, the thermal resistance of the PCM considering the fraction of the melted PCM is expressed as the sum of the resistance of the PCM solid layer and the PCM liquid layer and is expressed as follows:

$$R_{PCM} = \log\left(\frac{\left(f \ \left(R_5^2 - R_4^2\right) + R_4^2\right)^{0.5}}{R_4}\right) \frac{1}{2\pi L_{he} k_{PCM,L}} + \log\left(\frac{R_5}{\left(f \ \left(R_5^2 - R_4^2\right) + R_4^2\right)^{0.5}}\right) \frac{1}{2\pi L_{he} k_{PCM,S}} \quad \textbf{(24)}$$

Total heat transfer rate Q_w, the total heat transferred to the water is assumed equal to the total useful heat Q_u minus the heat transferred to the PCM $Q_{PCM,c}$:

$$Q_w = Q_u - Q_{PCM,c} \quad (25)$$

3.2.2 Discharging the PCM

The heat transferred from water in the middle tube to the PCM is expressed as follows:

$$Q_{PCM,d} = \varepsilon_d C_{min} \left(T_{PCM} - T_{c,in}\right) \quad (26)$$

With ε_d the average effectiveness of the solidification process is expressed as follows:

Total heat transfer rate Q_w, the total heat transferred to the cold water is assumed equal to the sum of the heat released from the PCM $Q_{PCM,d}$ and the useful heat Q_u :

$$Q_w = Q_{PCM,d} + Q_u \quad (27)$$

3.3 Definition of the system performance

The energy efficiency of the system is characterized by two main parameters:

- ✓ The overall thermal efficiency η_o of the PVT module, that is the sum of the electrical efficiency η_e and the thermal efficiency η_{th} of the system.

$$\eta_o = \eta_e + \eta_{th} \quad (28)$$

- ✓ The COP (Coefficient Of Performance) The coefficient of performance (COP) of the system could be defined as the ratio of system's overall heat output (including the power output converted to heat) and power consumption of the water pump as following [19]:

$$COP = \frac{Q_w + Q_e/0.38}{P_{pump}} \quad (29)$$

The electricity consumption of the pump is expresses as follows:

$$P_{pump} = \frac{Q_v \, \rho_w g \, H}{\eta_{pump}} \quad (30)$$

Where Qv is the water volume flow rate, η_{pump} the efficiency of the pump and H the total height H expressed as following:

$$H = f_{an} \frac{L_{he}}{D_3 - D_2} \left(\frac{u_w^2}{2\,g}\right) + \sum K \left(\frac{u_w^2}{2\,g}\right) \quad (31)$$

Where f_{an} is the friction factor for an annular tube given in Annex 3 and $\sum K$ is the sum of loss coefficient for the four 180 returned bend, inlet and outlet fittings [25].

3.4 Presentation of the algorithm of the integrated model of the PVT system

The global model is resolved by ensuring the heat balance at the micro-channel evaporator and at the PCM heat exchanger. The algorithm is summarized in Fig. 6.

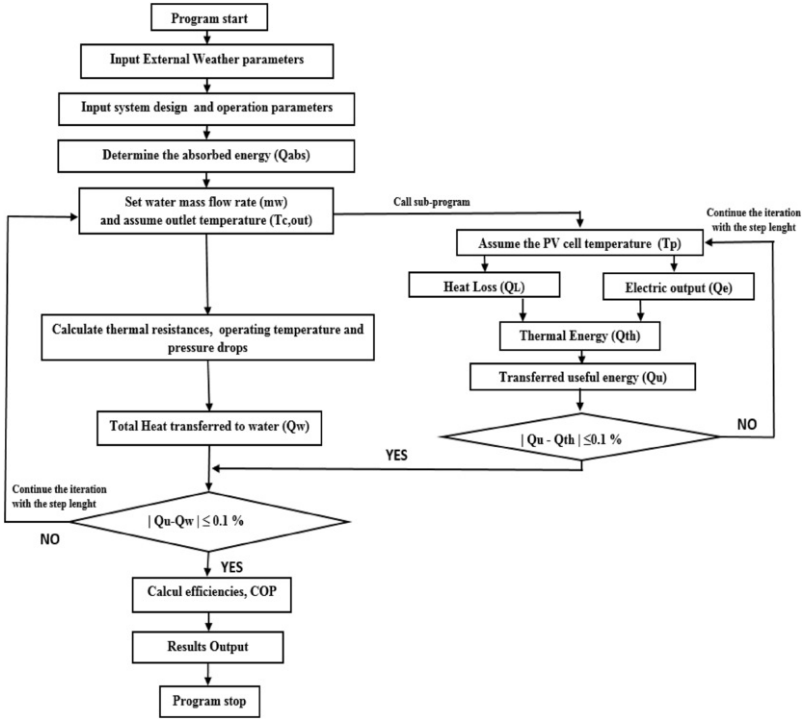

Fig. 6 PV/LHP thermal performance model.

alt-text: Fig. 6

The algorithm is illustrated as follows:

(i) Input external weather variables, system design and operating parameters;

(ii) Calculate the Absorbed heat equation (A.1) (Annex 1)

(iii) Set the cold water mass flow m_w rate and the water inlet temperature $T_{c,int}$

(iv) Assume the outlet temperature of the water $T_{c,out}$.

(v) Calculate the total heat transfer rate Q_w Equation (25) (Charge process) or 27 (Discharge process).

(vi) Assume the cell temperature Tp, and commence the following analysis:

A. Heat balance of the glazing cover could be analysed using equations A.2 to A.12, which gives the heat loss, QL;

B. Heat balance of the PV cells gives of the converted solar electricity, Q_e and heat, Q_{th}; (A.10 and A.12).

C. Heat transfer from the PV cells to the PCM heat exchanger could be analysed by Equations (1)-(17), which gives the useful heat gain, Q_u;

D. If $(Q_{th} - Q_u)/Q_{th} > 0.1\%$ (error allowance), then increase tp by 0.1 °C and return to step (vi) for re-calculation;

E. If $(Q_{th} - Q_u)/Q_{th} < -0.1\%$ (error allowance), then decrease tp by 0.1 °C and return to step (vi) for re-calculation;

F. If $-0.1\% \leq (Q_{th} - Q_u)/Q_{th} \leq 0.1\%$, the system achieves heat balance;

(vii) If $(Q_u - Q_w)/Q_u > 0.1\%$ (error allowance), then increase $T_{c,out}$ by 0.1 °C and return to step (iii) for re-calculation;

(viii) If $(Q_u - Q_w)/Q_u < -0.1\%$ (error allowance), then decrease 0.1 °C and return to step (iii) for re-calculation;

(ix) If $-0.1\% \leq (Q_u - Q_w)/Q_u \leq 0.1\%$, the system achieves heat balance;

(x) Calculate the module's energetic efficiencies and the overall performance coefficient of $COP_{PV/T}$ using Equations (28)-(31) and the program stops.

3.5 Parametric study on the energy efficiency od the new PVT system

In this part, the established computer model has been used to study the influence of the following parameters on the energy performance of the system:

- ✓ the weather conditions (external parameters: solar radiation, ambient temperature, wind velocity)
- ✓ the system configuration (internal parameters: cover number, packing factor, number of heat pipes),
- ✓ the working fluid characteristics (water inlet temperature, water mass flow rate).

3.5.1 Influence of the solar radiation

By varying the solar radiation from 200 W/m^2 to 800 W/m^2 while keeping other external variables constant, i.e. air temperature at 25 °C, air velocity at 1 m/s, the energy performance of the is assessed. The PCM is assumed to have a melting temperature of 44 °C. Fig. 7a shows the influence of the solar radiation I on the thermal η_{th}, electrical η_e and overall η_o efficiencies. The increase of the solar radiation would lead to an increase of the thermal and overall efficiency and a decrease of the electrical efficiency. The thermal efficiency outweighs the electrical efficiency and thus the overall efficiency follows this increasing trend. The increase is most significant for relatively lower solar radiations ($I < 400$ W/m^2) and is almost linear. It can be found that the trend increases rapidly in 200–400 W/m^2 range; however, it slows down above a solar radiation of 400 W/m^2. For each 100 W/m^2 increase the overall efficiency increases by nearly by 7% and by 1.6% for the slow trend. The slow trend is due to the increase of the water outlet temperature, therefore there is heat loss from the panel to the ambient air while increasing the solar radiation. For a solar radiation of 800 W/m^2 the PVT module reaches an overall efficiency of 67.8%. The increase of the solar radiation from 200 W/m^2 to 800 W/m^2, actually leads to a small decrease (0.28%) of the electrical efficiency from 12.48 to 12.2%. This is because the higher solar radiation brings more instant heat to the PV layer, resulting in an increase of the PV cell temperature as shown in Fig. 7b and the decrease of the electrical efficiency. For a solar radiation of 800 W/m^2 the PVT module reaches an overall efficiency of 67.8%.

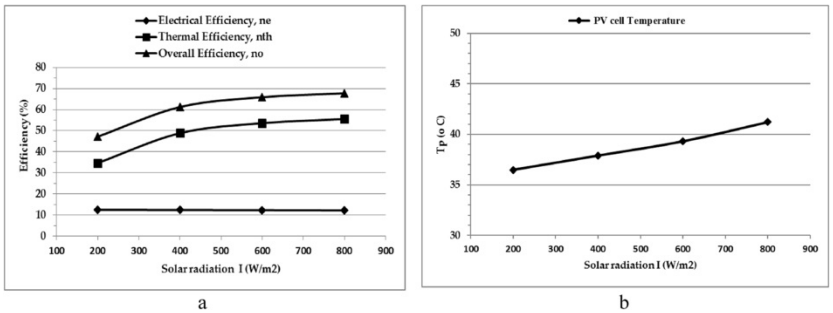

Fig. 7 Influence of solar radiation on: a) the thermal, electrical, overall efficiencies, b) PV cell temperature.

alt-text: Fig. 7

Fig. 8a presents the influence of the solar radiation on the useful heat Q_u transferred to the circulating water temperature, the total heat transferred Q_w to the network/heat storage tank and Q_{pcm}. Increasing the solar radiation would increase the useful Q_u heat and therefore the total heat transferred to the circulating water the Q_w. The heat released (discharged) by the PCM Q_{PCM} and transferred to the water is constant, as the calculation has been performed for an assumed constant PCM temperature of 44 °C (Equation (25)). The amount of heat released by the PCM is 110 W. The contribution of the PCM release in the total heat transfer rate decreases as the solar radiation increases. For the solar radiation of 200 W/m^2, the heat from the PCM Q_{PCM} represents 43% of the total heat transfer rate ($Q_w = 256$ W) and this percentage is 11% ($Q_w = 987$ W) for higher solar radiation of $I = 800$ W/m^2. It is seen that the presence of the PCM produces an increase in the total heat transfer rate wick, which is more important at lower solar radiations. Increasing the solar radiation by 100 W/m^2 would increase the water output temperature by 1.33 °C (Fig. 8b). For a solar radiation of 800 W/m^2, the system delivers a water temperature of 45.8 °C.

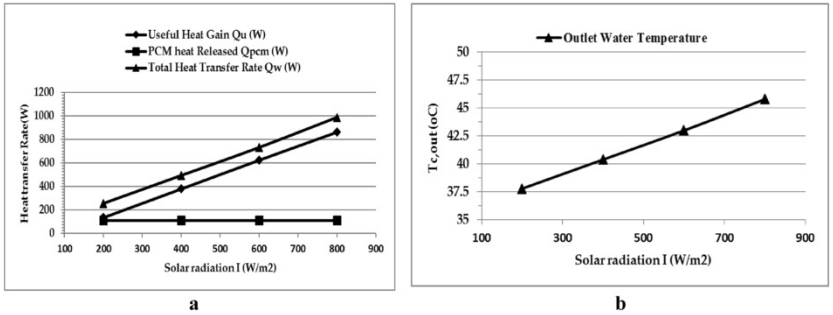

Fig. 8 Influence of solar radiation on a) the heat outputs and b) the water outlet temperature.

alt-text: Fig. 8

Fig. 9 presents the influence of the solar radiation the COP of the PVT system which considers both electrical and thermal outputs (Equation (28)). The COP increases linearly with the solar radiation. The high COP value (2–3 order) reflects the small power consumption of the pump. The increase of solar radiation significantly influences the COP which is multiplied by 4.3 when the solar radiation increases from 200 W/m^2 to 800 W/m^2. The solar radiation increase is very beneficial to the PVT system.

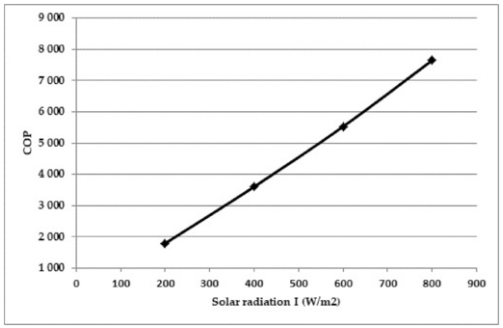

Fig. 9 Influence of solar radiation on the COP.

alt-text: Fig. 9

3.5.2 Influence of the ambient temperature

Varying the air temperature from 5 °C to 35 °C while the other external variables remained constant, i.e. solar radiation at 800 W/m^2, air velocity at 1 m/s, PCM melting temperature of 44 °C, the energy performance of the system was assessed. Fig. 10a shows that increasing the ambient temperature would increase the thermal and the overall efficiency but decrease the electrical efficiency. As the thermal efficiency outweighs the electrical efficiency, the overall efficiency follows the thermal efficiency which increases linearly. For each 5 °C ambient temperature increase the overall efficiency increases by 4%. From 5 °C to 35 °C ambient temperature, the electricity efficiency decreases slightly because the PV cell temperature rose 2.58 °C, from 39.3 °C to 41.9 °C as shown in Fig. 10b. This small increase of the PV cell tell temperature can be explained by the high capacity of the micro-channel evaporator to absorb heat flux, the two-phase heat transfer coefficient in the microchannel evaporator is in the order of 4×10^3 $W/m^2/K$ and by the heat loss decrease when increasing the ambient temperature.

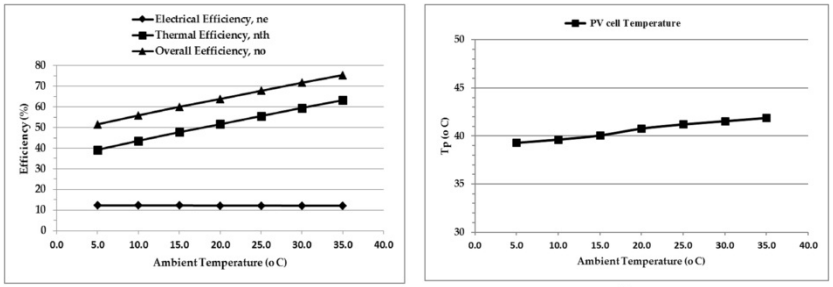

Fig. 10 Influence of the ambient air temperature on: a) the thermal, electrical, and overall efficiencies, b) PV cell temperature.

alt-text: Fig. 10

Fig. 11a presents the evolution the heat output rates and the circulation water outlet temperature at the PCM heat exchanger. A higher ambient temperature would lead to higher total heat transfer rate Q_w. At 35 °C, the system achieves a total heat transfer rate of 1096 W. Fig. 11b shows that from 5 °C to 35 °C ambient temperature, the water outlet temperature increases by 4 °C, this means for each 7.5 °C ambient temperature increase the water outlet temperature increases by 1 °C.

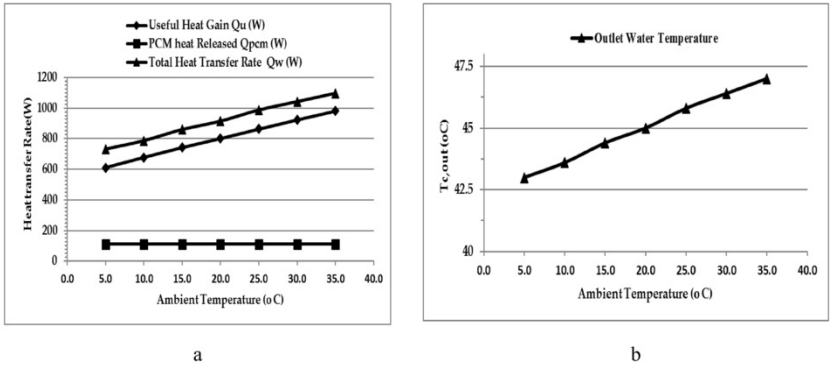

Fig. 11 Influence of the ambient temperature on a) the heat outputs and b) the water outlet temperature.

alt-text: Fig. 11

Fig. 12 presents the influence of the ambient temperature on the COP. The COP of the system increases linearly with the increase of the ambient temperature due the linear increase of the total heat transferred to the water Q_w. The temperature increase is a favourable factor on the COP that is multiplied by 1.34 when the ambient temperature increases from 5 °C to 35 °C. It can be seen that the influence of the solar radiation on the COP (Fig. 9) is stronger than the influence of the ambient temperature (Fig. 12).

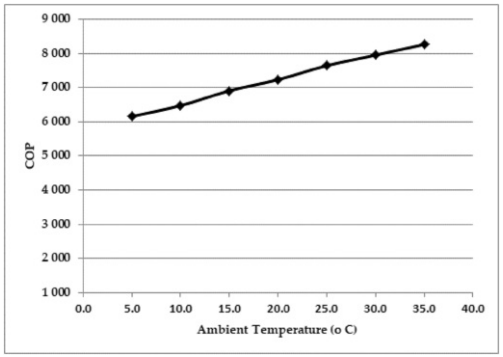

Fig. 12 Influence of ambient temperature on the COP.

alt-text: Fig. 12

3.5.3 Influence of the wind velocity

Varying the wind velocity from 0.5 m/s to 5 m/s while maintaining the other external variables constant values, i.e. solar radiation at 800 W/m^2, air temperature at 25 °C, the energy performance of the system has been assessed. It was found that increasing wind velocity would slightly decrease the overall efficiency and very slightly increase the electricity efficiency (Fig. 13a). Increasing the wind velocity by 1 m/s decreases the overall efficiency by 0.3% (from 67.9 to 66.5%). This decrease is due to the small increase of the system heat loss due to the increase of the convective heat transfer coefficient from the PV to the surroundings. However, this heat transfer coefficient is favourable for the electricity efficiency which increases very slightly (almost constant) from 12.2 to 12.21%. As shown in Fig. 13b, the wind velocity increase led to a very slight decrease in the temperature of the PV cells (40.58 °C–40.39 °C). This PV cell temperature decrease is favourable to the system but the effect is weak.

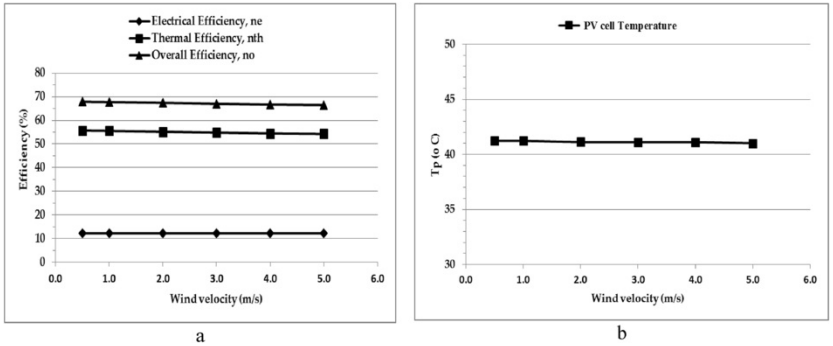

Fig. 13 Influence of the wind velocity on the a) the thermal, electrical, and overall efficiencies, b) PV cell temperature.

alt-text: Fig. 13

Fig. 14 presents the influence of the wind velocity on the total heat transfer rate and the water outlet temperature. Increasing the wind velocity by 1 m/s slightly decreases the total heat transfer rate Q_w by 0.8% (Fig. 14 a) and the water outlet temperature $T_{c,out}$ by 0.08 °C (Fig. 14 b).

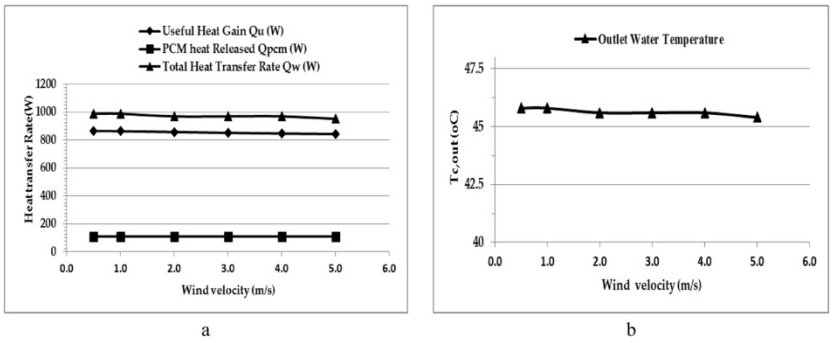

Fig. 14 Influence of wind velocity on: a) the heat outputs and b) the water outlet temperature.

alt-text: Fig. 14

Fig. 15 shows that COP decreases slightly with an increasing air velocity. Increasing the velocity from 0.5 m/s to 5 m/s decreases the COP by 4%. It can be seen that the influence the wind velocity on the COP of the system is very weak compared to the influences of the solar radiation (Fig. 9) and the ambient temperature (Fig. 12).

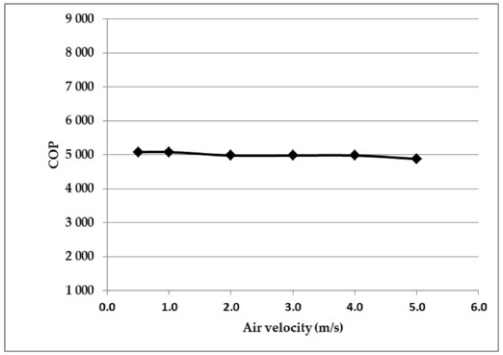

Fig. 15 Influence of wind velocity on the COP.

alt-text: Fig. 15

3.5.4 Influence of number of cover

By varying the number of top glazing covers from 0 to 2 while the other parameters remained constant, i.e. solar radiation at 800 W/m^2, air temperature at 25 °C, velocity 1 m/s, it was found that increasing the number of glazing covers would increase the thermal, and slightly decrease the electrical, efficiency (Fig. 16a). As the thermal efficiency overweighs the electrical efficiency, the overall efficiency follows the thermal efficiency increase. The increases of the overall efficiency can be explained by the fact the adding more glazing covers helps to reduce the overall heat losses and the amount of absorbed solar energy due to its reflection and reduced transmittance; therefore, the thermal efficiency and the PV cell temperature rises slightly from 39.2 to 40.9 °C (Fig. 16b), and then the electrical efficiency falls slightly (12.19%–12.17%). The increase of the cover number is favourable for thermal efficiency and unfavourable for electrical efficiency.

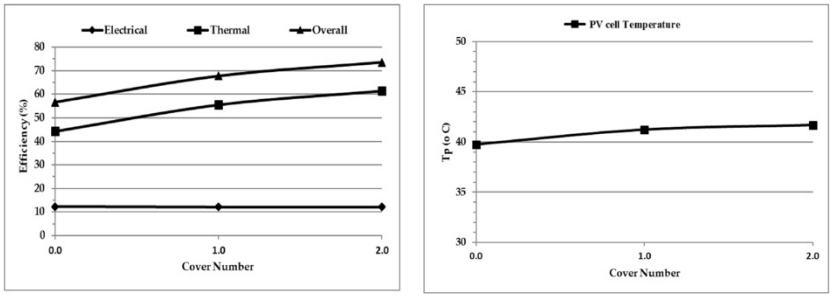

Fig. 16 Influence of the cover number on the efficiency.

alt-text: Fig. 16

Fig. 17 shows that increasing the number of covers from 1 to 2 increases the heat transfer rate by 7.3% (Fig. 17a) and water outlet temperature by 0.8 °C (Fig. 17b). Fig. 18 shows that the cover number is a favourable factor for the performance of the system. Increasing the number of covers from 1 to 2 causes the COP to increase by only 5.4% (Fig. 18), this means using 2 covers does not significantly increase the COP. To minimize heat loss and maximize solar energy input, the single-glazing cover was considered to be the most appropriate option.

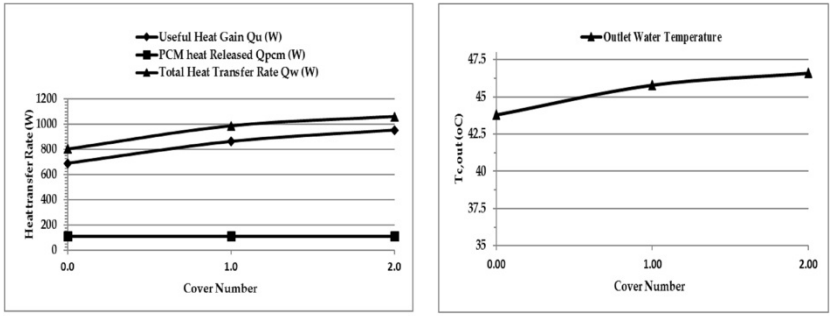

a b

Fig. 17 Influence of the cover number on heat transfer rates and the outlet water temperature.

alt-text: Fig. 17

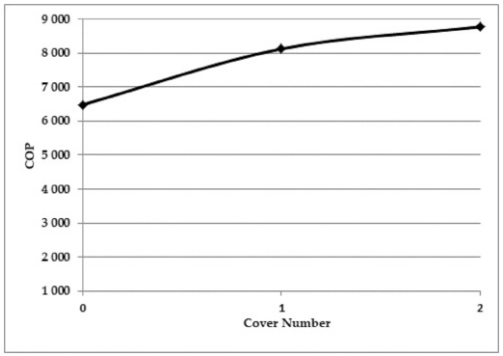

Fig. 18 Influence of the cover on the COP.

alt-text: Fig. 18

3.5.5 Influence of the packing factor

The influence of the packing factor on the energy performance of the system has been investigated for a constant solar radiation at 800 W/m^2, air temperature at 25 °C, wind velocity of 1 m/s. The packing factor has been varied by changing the number of PV cells. It was found that increasing the packing factor from 0.1 to 0.9 increases the overall efficiency from 60.4% to 67.7% (Fig. 19 a). This increase is in majority due to the significant increase of the electricity efficiency (1.5%–12.2%), the thermal efficiency decreases less (58.9%–55.5%). Fig. 19b shows that the increase of the packing factor slightly influences the PV cell temperature. The packing is significantly favourable to the electricity efficiency and unfavourable to the thermal efficiency.

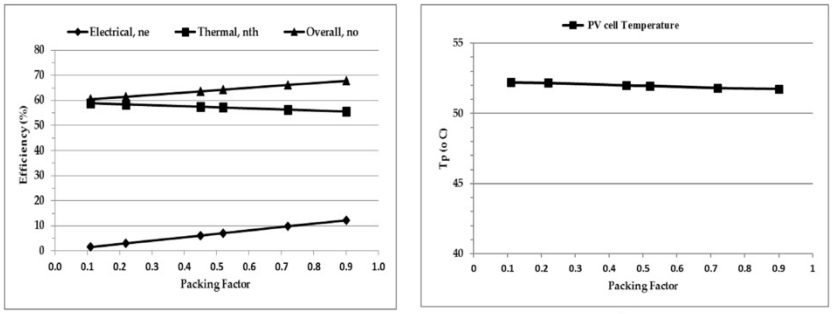

a b

Fig. 19 Influence of the packing on the efficiency.

alt-text: Fig. 19

Fig. 20 shows that total heat transferred to the water $Q_{w,}$ and the outlet water temperature, decreases slightly with the packing factor. As a result, from a packing factor of 0.1–0.9 the COP decreases slightly by 36.5% (Fig. 21). In fact, this increase of the COP is due to the increase of the electrical output that compensates the small decrease of the total heat output. Finally, it was found that higher packing factor is beneficial for the overall system performance.

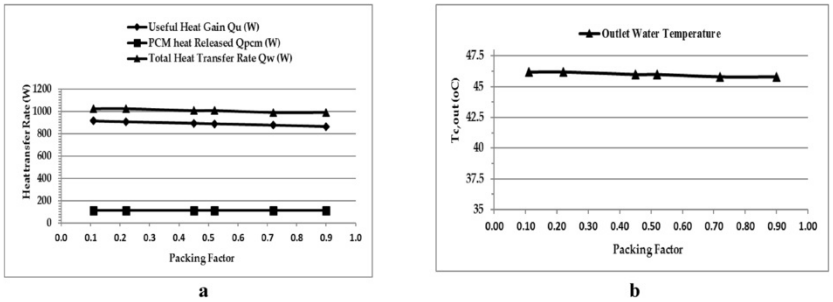

a

b

Fig. 20 Influence of the packing factor on heat transfer rates and the outlet water.

alt-text: Fig. 20

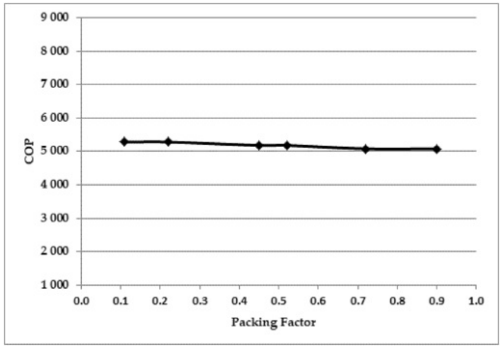

Fig. 21 Influence of the packing factor on the COP.

alt-text: Fig. 21

3.5.6 Influence of number of heat pipe

By varying the number of heat pipes from 5 to 10 while the other parameters remained constant, solar radiation at 800 W/m^2, air temperature at 25 °C, a wind velocity of 1 m/s. It was found that increasing the number of microchannel heat pipes increases the overall efficiency of the system from 64.9% to 67.85% (Fig. 22a) and the effect is most evident for heat pipe quantities less than 10. It is found that for a microchannel heat pipe number (N_{hp}) superior to 20 the overall heat transfer coefficient is approximately constant (Fig. 22a). The total heat transfer rate tends also to be constant. Fig. 23 shows also that for Nhp>20, the PV cell and the outlet water temperatures, 40.48 °C and 45.8 °C respectively, are constant. The COP of the system also follows this behaviour (Fig. 24) and is constant for a N_{hp} superior to 20. This means that 20 microchannel heat pipes represent an optimal microchannel number.

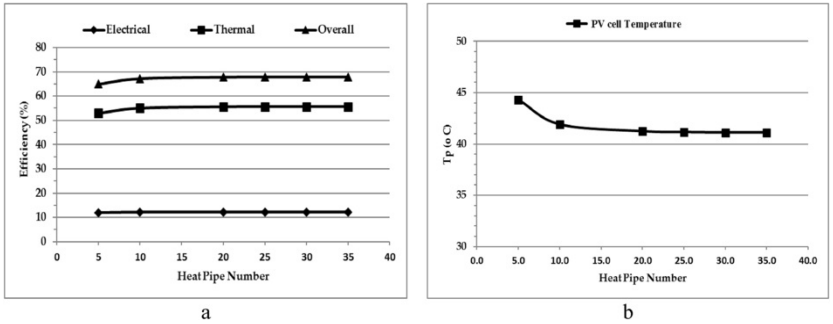

a b

Fig. 22 Influence of the microchannel heat pipe number on the efficiency.

alt-text: Fig. 22

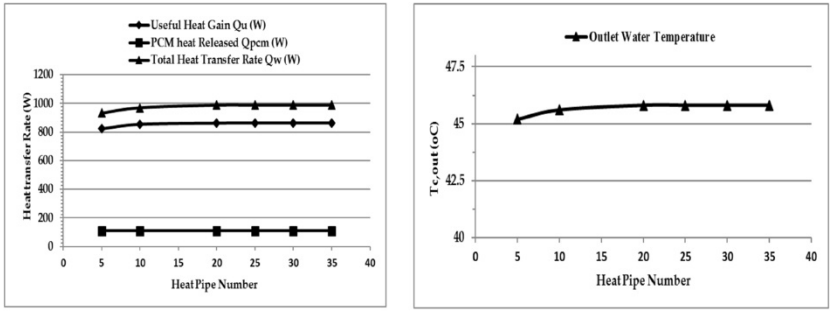

a b

Fig. 23 Influence of microchannel the heat pipe number on the PV cell temperature and the outlet water temperature.

alt-text: Fig. 23

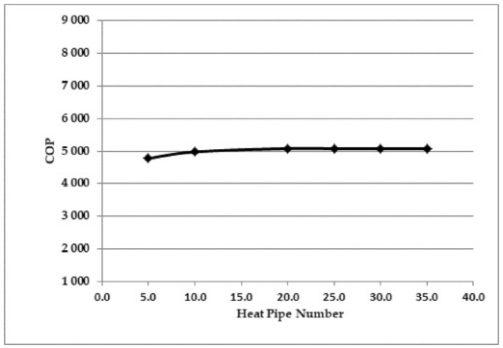

Fig. 24 Influence of microchannel heat pipe number on the COP.

alt-text: Fig. 24

3.5.7 Influence of water inlet temperature

By varying the cold water inlet temperature at the heat exchanger from 20 °C to 40 °C. While the other parameters remained constant solar radiation at 800 W/m^2, air temperature at 25 °C, wind velocity at 1 m/s. It was seen that increasing the water inlet temperature would significantly decrease the overall efficiency of the system (Fig. 25a). This decrease in due to the increase of the water outlet temperature (Fig. 26b) which increases the heat loss in the loop system. Fig. 25a shows that an

increase of the water inlet temperature significantly decreases the total heat transfer rate. This significant decrease is due to the decrease of the useful heat Q_u because of the heat loss increase and the decrease of the total heat released the PCM Q_{cm}. It can be seen that for a water inlet temperature near 38 °C the useful heat Q_u is superior to the total heat transfer rate Q_w (Fig. 25b). This means there is excess heat is charged in the PCM.

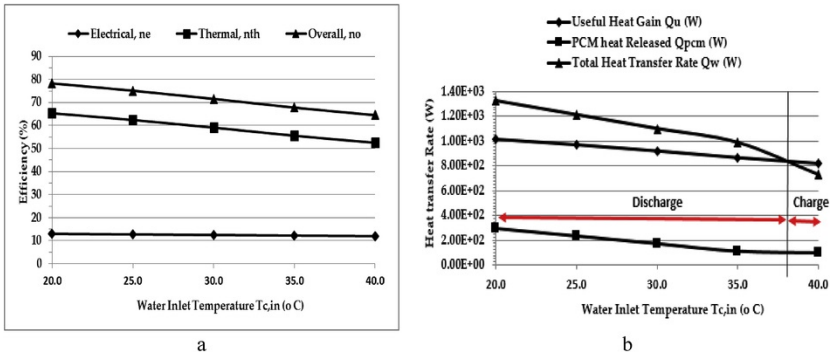

Fig. 25 Influence of the water inlet temperature on the efficiency.

alt-text: Fig. 25

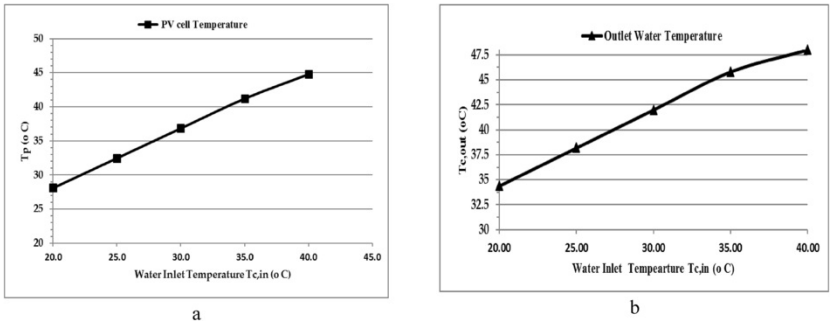

Fig. 26 Influence of the water inlet temperature on heat transfer rates and the outlet water.

alt-text: Fig. 26

Fig. 27 shows that the COP evolution presents a maximum value where the heat excess is beginning to be charged in the PCM and the COP falls.

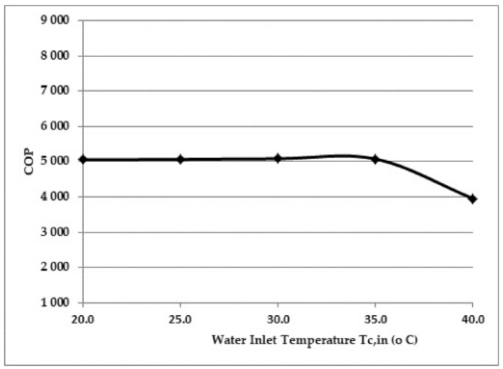

Fig. 27 Influence of the water inlet temperature on the COP.

alt-text: Fig. 27

3.5.8 Influence of the water mass flow

By varying the water mass flow rate from 0.01 to 0.087 kg/s, while the other parameters remained constant, the influence of this factor on the system performance was assessed. For lower mass flow rates $m_w < 0.04$ m/s, the overall efficiency of the module increases with the flow rate, after this point the efficiency tends to be constant (Fig. 28a). This can be explained by the fact that increasing the mass flow rate decreases the mean temperature of the water in the annular tube which decreases the heat losses in the system. Consequently, the useful heat gain increases (Fig. 29b) and the thermal efficiency increases. The electrical efficiency also increases because of the PV cell temperature decreases (Fig. 28b). Otherwise the increase of the mass flow rate decreases the heat released by the PCM for flow rate inferior to 0.02 kg/s, while above this tends to be constant. Fig. 30 shows that the increase of the mass flow rate significantly influences the COP of the system, because of the supplementary electricity consumption of the system. It is seen that the flow rate of 0.0125 kg/s would be an optimal value for high COP and high heat output simultaneously.

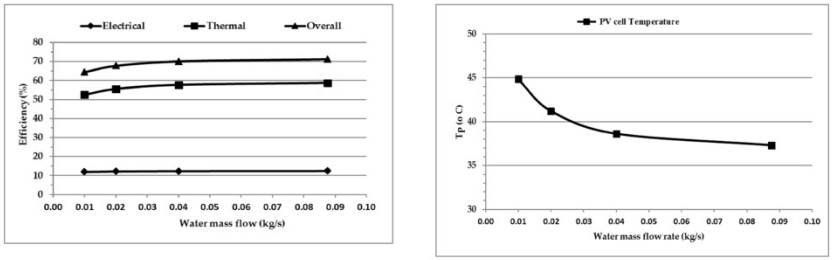

a b

Fig. 28 Influence of the water mass flow rate on heat transfer rates and the outlet water.

alt-text: Fig. 28

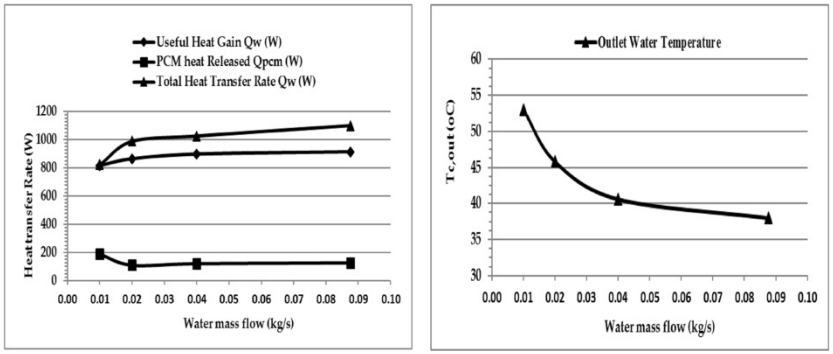

a b

Fig. 29 Influence of the water mass flow rate on the efficiency.

alt-text: Fig. 29

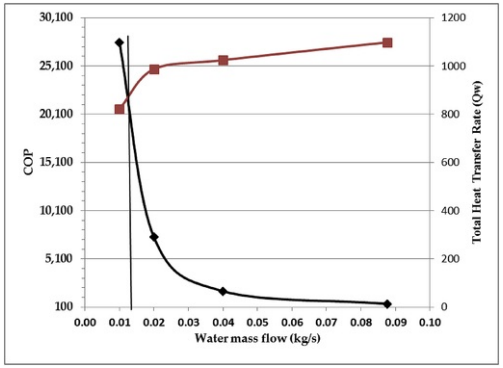

Fig. 30 Influence of the water mass flow rate on the COP.

alt-text: Fig. 30

3.6 Comparision of the novel system with a conventional system

In this section the novel PVT system has been compared with a conventional system (Fig. 31). The conventional system has a hydraulic diameter of 12 mm (vs 1.2 mm for the novel system) and the loop heat pipe has a flat plate heat exchanger for the condensation. The model of the plate heat exchanger is described in Ref. [26]. For the conventional system, the liquid return enters at the bottom of the system. For each system the same number (20) of heat pipe collectors has been supposed. For the two systems the same PV and glazing cover optical and thermal properties were used (Annex 1). The efficiency of these systems was assessed for an ambient temperature of 25 °C and a wind velocity of 1 m/s.

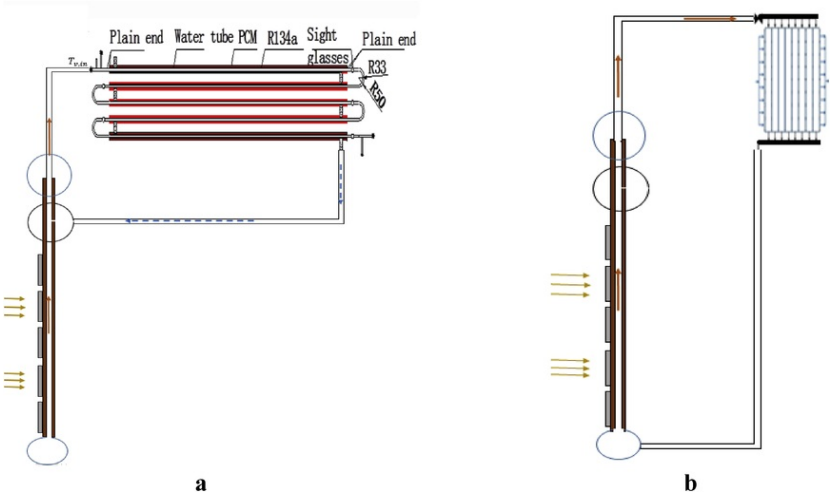

Fig. 31 Comparison between, a) the novel PVT system b) the conventional PVT system.

alt-text: Fig. 31

Fig. 32 shows the efficiency of the system for different solar radiation intensities and the resulting efficiency increases. Compared to the novel system, the system efficiency increases at least by 33% for the thermal efficiency, 8.7% for the electrical efficiency and 28.8% for the overall efficiency. The efficiency increase is more important at lower solar radiations. This performance is due to three main factors: Firstly, a higher heat transfer rate in the micro-channel evaporator that absorbs more heat (4340 $W/m^2/K$ against 1500 $W/m^2/K$), secondly the significant decrease of the PV cell temperature (e.g. decrease of 12.31 °C at 800 W/m^2) and finally because of the heat released by the PCM heat exchanger.

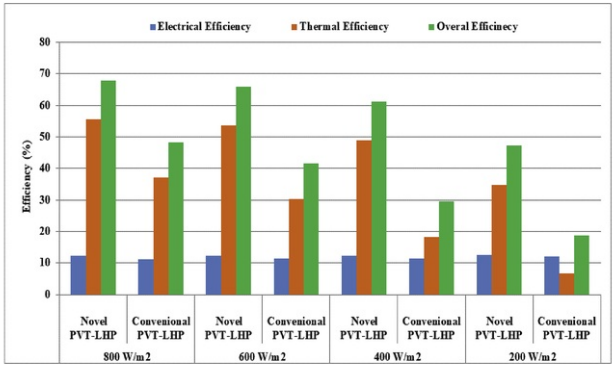

a

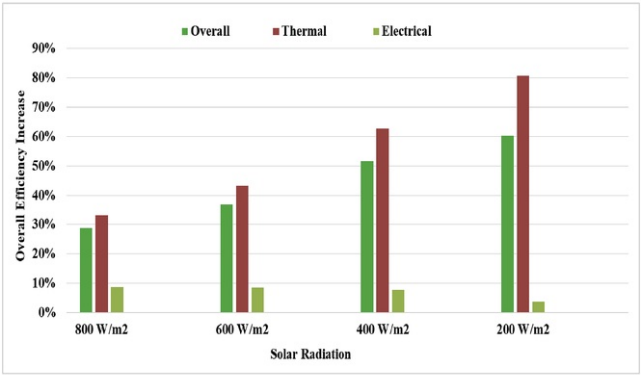

b

Fig. 32 Comparison between the new PVT system and the conventional PVT system a) evolution of thermal, electrical, overall efficiencies b) overall efficiency increase.

alt-text: Fig. 32

Fig. 33 shows the COP of the system for different solar radiation intensities and the COP ratio of the novel system to the conventional system. It was found that the overall COP of the system was at least 2.2 times higher when compared to the conventional system. This higher COP is due to the higher heat output of the novel system and the lower power consumption of the water pump (0.18 W against 0.12 W).

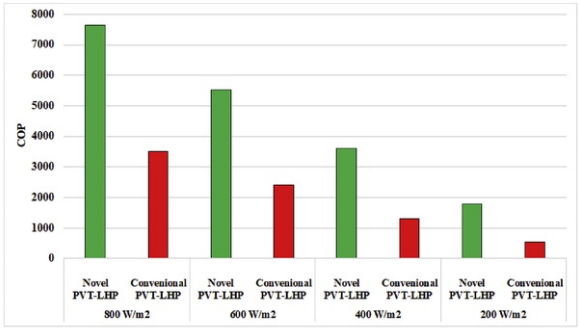

a

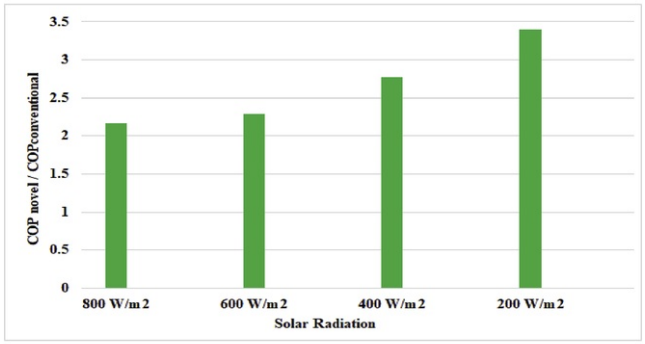

b

Fig. 33 Comparison between the new PVT system and the conventional PVT system a) evolution of the COP and b) the ratio of COP novel to COP conventional.

alt-text: Fig. 33

3.7 Comparision between the novel PV/T-LHP system efficiency and experimental efficiency of PVT systems from the literature

Table 2 shows the summarized comparison results between the proposed PVT-LHP system efficiency and experimental efficiency of PVT systems reported in the literature [30–36]. From Table 2, it can be found that the overall efficiency of the developed PVT-LHP system at design conditions (this design conditions are based on the authors' previous experiment results [11] and conditions) is higher than the reported efficiencies of PVT systems with natural circulation (NC) and systems assisted by Heat Pumps (HP). This means, if the theoretical efficiency of the novel system is confirmed by experiments, the development of the novel PVT-LHP system is promising.

Table 2 Comparison of the novel system efficiency and the experimental efficiency of PVT systems in the literature.

alt-text: Table 2

Solar radiation (W/m²)	Electrical Efficiency (%)	Thermal efficiency (%)	Overall efficiency (%)	Reference
800	12.2	55.6	67.8 5 (NC)	Present study
800	7.9	54	61.9 (with HP assistance)	[30] (Fig. 12 Q_m = 0,03 kg/s)
800	11.3	54	65.3 (with HP assistance)	[31]
Daily average	9.13	39.25	48.37 (HP assistance)	[32]
Summer (value not indicated)	5.39	31.58	36.97 (NC)	[33]
–	11	51	62 (NC)	[34]

Daily average	9.87	40	49.87 (NC)	[35]
Daily average	10.15	45	55.15 (NC)	[36]

4 Conclusion

This paper presented a novel solar PVT Loop Heat Pipe (PVT-LHP) system using a Micro-channel evaporator and a PCM triple heat exchanger. A computer model was developed to assess the performance of the PVT-LHP system on the basis of a heat balance mechanism, which gave the predicted PV modules' solar thermal, electrical and overall efficiencies, and the system's overall performance coefficient ($COP_{PV/T}$) at the specified operational conditions. The influence of the environmental parameters (i.e. solar radiation, air temperature, wind velocity), structural parameters (i.e. glazing covers, number of the absorbing heat pipes, PC cell packing factor), the variable inputs (i.e. water inlet temperature, mass flow rate) on the energy performance of the system was investigated individually. The novel PVT-LHP has been compared with a conventional Solar PVT-LHP system. It was found that:

(1) Increasing the solar radiation led to an increase in thermal efficiency but a decrease in the electrical efficiency, resulting in an increase the system's overall performance coefficient ($COP_{PV/T}$);

(2) Increasing the ambient air temperature led to an increase in the thermal efficiency, a decrease in the electrical efficiency and an increase in the system's overall performance coefficient ($COP_{PV/T}$);

(3) Increasing the wind speed led to a slight decrease in the thermal efficiency, slight increase in the electrical efficiency and slight decrease in the system's overall performance coefficient ($COP_{PV/T}$);

(4) Increasing the number of the glazing covers led to an increase in the module's thermal efficiency but a decrease in the module's electrical efficiency and in the system's overall performance coefficient ($COP_{PV/T}$)

(5) Increasing the packing factor led to a decrease in the module's thermal efficiency but an increase in the module's electrical efficiency and in the system's overall performance coefficient ($COP_{PV/T}$)

(6) Increasing the number of the heat absorbing pipes led to an increase in the fin's efficiency and in the system's overall performance coefficient.

(7) Increasing the cold water inlet temperature led to a decrease in the module's thermal efficiency, the module's electrical efficiency, and the system's overall performance coefficient ($COP_{PV/T}$).

(8) Increasing the water mass flow rate led to an increase in the module's thermal efficiency and the module's electrical efficiency, and in a decrease the system's overall performance coefficient ($COP_{PV/T}$) because of the increase of the pump electricity consumption. The results show that a flow rate of 0.0125 kg/s would be an optimal flow for a high Heat output and high COP simultaneously.

Furthermore, on the whole, the increase of solar radiation, ambient temperature, cover number, heat pipe number, and packing factor are determined to be the favourable factors for the $COP_{PV/T}$ (Coefficient Of Performance) of the system, whereas higher wind velocity and cold water mass flow rate have been observed to be unfavourable. Under the given design conditions, a number of micro-channel heat pipes of 20 and one glazing cover was found optimal. The electrical, thermal and overall efficiency of the PVT-LHP module were found 12.2%, 55.6% and 67.8% respectively and can achieve 28% higher overall energy efficiency and 2.2 times higher overall coefficient of performance $COP_{PV/T}$ compared to the conventional system. The model developed in this study can be used to design and optimize the energy performance of a novel PVT-LHP system.

Acknowledgments

The authors would acknowledge our appreciation to the financial supports from the EPSRC (EP/R004684/1) and Innovate UK (TSB 70507-481546) for the Newton Fund – China-UK Research and Innovation Bridges Competition 2015 Project ‘A High Efficiency, Low Cost and Building Integrate-able Solar Photovoltaic/Thermal (PV/T) System for Space Heating, Hot Water and Power Supply’ and DongGuan Innovative Research Team Program (No. 2014607101008).

Annex 1 characteristics of different PVT layers

Parameters	Nomenclature	Value	Unit
Emissivitiy of glazing cover	ε_c	0.84	[−]
Absorptance of glazing cover	A_c	0.05	[−]
Transmittance of glazing cover	τ_c	0.90	[−]
Emissivitiy of PV cell	ε_{abs}	0.96	[−]
Absorptance of PV cell	α_{abs}	0.90	[−]

Thickness of PV Cell	δ_{abs}	0.0003	m
Thermal conductivity of PV cell	λ_{abs}	148	W/m/K
Reference efficiency of PV Cell	η_{rc}	0.18	[−]
Temperature coefficient of PV cell	β_{abs}	0.0045	1/°C
Reference temperature of PV cell	trc	25	° C
Number of PV cell	N_{pv}	72	[−]
Area of single PV cell	A_{pv}	0.156*0.156	m^2
Thickness of EVA grease	δ_{eva}	0.0005	m
Thermal conductivity of EVA grease	λ_{eva}	0.35	W/m/K
Thickness of electrical insulation	δ_{ei}	0.002	m
Thermal conductivity of electrical insulation	λ_{ei}	144	W/m.K
Absorptance of blacken electrical insulation	A_{ei}	0.8	[−]
Thickness of fin sheet	δf	0.005	[−]
Thermal conductivity of fin sheet	λ_f	203	[−]

Annex 2 heat transfer from outside to the PV surface [19].

The solar energy received by the PV module is expressed as follows:

$$Q_{abs} = \tau_c^{N_C} \tau_{g,pv} \left[\alpha_p \beta_p + \alpha_b \left(1 - \beta_p\right)\right] A_m I \quad \textbf{(A2.1)}$$

where, τ_c and $\tau_{g,pv}$ are the visual transmittances of cover plate and the glazing layer of PV lamination respectively; N_c is the number of cover plates; αabs and α_b are the absorption ratios of the PV layer and its baseboard; β_p is the packing factor of PV layer; A_m is the collector area of the module (m^2). The loss heat from a double-glazed module will experience (1) heat transfer from the PV absorber surface to the inner glazing cover; (2) heat transfer from the inner cover to the outer cover; and (3) heat transfer from the outer glazing cover to the ambient air. As shown in the following figure, the three forms of heat transfer are laid in a series and achieve a balance.

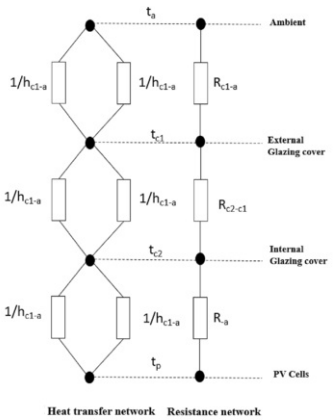

Thermal network of heat loss for a typical double-cover module

alt-text: Image 2

Therefore, the total heat loss is written as:

$$Q_L = U_L A_m \left(T_p - T_a\right) \quad \textbf{(A2.2)}$$

Where, Q_L and U_L are the total heat loss (W) and the heat loss coefficient (W/m^2-K) respectively; T_p and T_a are the average temperatures of PV layer and the ambient air (K). Where the U_L is the overall heat transfer coefficient and could be written:

$$U_L = \left(\frac{1}{h_{c,p-c2} + h_{R,p-c2}} + \frac{1}{h_{c,c2-c1} + h_{R,c2-c1}} + \frac{1}{h_{c,c1-a} + h_{R,c1-a}}\right)^{-1} \quad \textbf{(A2.3)}$$

where, $h_{c,p-c2}$, $h_{c,c2-c1}$ and $h_{c,c1-a}$ are respectively the convective heat transfer coefficients (W/m^2 -K) of PV layer (p) to inner cover surface (c2), inner cover surface (c2) to external cover surface (c1) and external cover surface (c1) to ambient air (a); $h_{R,p-c2}$, $h_{R,c2-c1}$ and $h_{R,c1-a}$ are the radiative heat transfer coefficients (W/m^2 -K) of PV layer (p) to inner cover surface (c2), inner cover surface (c2) to external cover surface (c1) and external cover surface (c1) to ambient air (a) respectively.

$$h_{c,p-c2} = \frac{k_{a,p}}{\delta_{a,p}} \left\{ \begin{array}{l} 1 + 1.446\left(1 - \frac{1708}{Ra_{a,p}\cos\theta}\right)^{+}\left[1 - \frac{1708\sin(1.8\theta)^{1.6}}{Ra_{a,p}\cos\theta}\right] \\ \qquad + \left[\left(\frac{Ra_{a,p}\cos\theta}{5830}\right)^{0.333} - 1\right]^{+} \end{array} \right\} \quad \textbf{(A2.4)}$$

where, $k_{a,p}$ is thermal conductivity of air gap at the average temperature of PV layer and inner cover surface (W/m-k); $\delta_{a,p}$ is the PV layer to glazing cover distance (m); θ is the collector slop (degree); the bracket with plus means zero and positive values only; $Ra_{a,p}$ is the Rayleigh number of the air gap at PV layer and inner cover surface, given by:

$$Ra_{a,p} = \frac{g\left(T_P - T_{C2}\right)\delta_{a,p}^3}{v_{a,p}^2 T_{a,m}} Pr_{a,p} \quad \textbf{(A2.5)}$$

where, g is the gravitational acceleration (m/s^2) and ν_a is kinematic viscosity of air at the PV and inner cover surface (m^2/s); $Pr_{a,p}$ is the Prandtl number of the air gap at PV layer and inner cover surface, which is assumed to be independent of temperature and taken equal to 0.7; $T_{a,m}$ is the average air temperature of PV layer and inner cover surface which is

$$T_{a,m} = \frac{\left(T_P + T_{c2}\right)}{2} \quad \textbf{(A2.6)}$$

Where, T_p and T_{c2} are respectively the average temperatures (K) of PV layer and inner cover surface. Converting the radiation transfer into the equivalent convective one, a radiation-relevant factor, $h_{R,\,p\text{-}c2}$, is expressed by:

$$h_{R,p-c2} = \frac{\sigma\left(T_p + T_{c2}\right)\left(T_p^2 + T_{c2}^2\right)}{\left(\frac{1}{\varepsilon_p}\right) + \left(\frac{1}{\varepsilon_{c2}}\right) - 1} \quad \textbf{(A2.7)}$$

Where, T_{c1} is the average temperature of external cover surface (K); ε_p and ε_{c2} are emissivity of the PV layer and inner cover surface; σ is the Stefan – Boltzmann constant ($5.6679 \times 10\text{-}8\,W/m^2$ -K4).

Heat Transfer from the Inner Glazing Cover to the Outer Cover: Similarly, heat transfer from the inner glass to the outer glass can be calculated using equations (A.5) to (A.7) to substitute corresponding parameters, including temperature, air properties, and emissivity.

Heat Transfer from the Cover's Outer Surface to the Surrounding Air: For a surface exposed to the outside wind, the convective coefficient could be calculated using the Klein equation expressed as follows:

$$h_{c,c1-a} = \frac{8.6V^{0.6}}{L^{0.6}} \quad \textbf{(A2.7a)}$$

Where, V is the wind speed (m/s); L is the characteristic length of the collector (m). The minimum convective coefficient for a wind-exposed surface is considered to be 5 W/m^2 -K [7]; if the above calculation gives a lower value, this should be replaced by the minimum value since the temperature of the sky has little influence on the calculation result, it is usually represented by the air temperature, thus

$$h_{r,c1-a} = \varepsilon_{c1}\sigma\left(T_{c1} + T_a\right)\left(T_{c1}^2 + T_a^2\right) \quad \textbf{(A2.8)}$$

The PV cells' electrical efficiency is adversely proportional to their surface temperature and this dependency can be written as:

$$\eta_e = \eta_{rc}\left(1 - \beta_{PV}\left(T_p - T_{rc}\right)\right) \quad \textbf{(A2.9)}$$

The overall electricity output is, therefore, given as

$$Q_e = \eta_e \beta_p \alpha_p \tau_c^{N_c} \tau_{g,pv} I A_m \quad \textbf{(A2.10)}$$

The module's solar electrical efficiency could be calculated through

$$\eta_e = \frac{Q_e}{I A_m} \quad \textbf{(A2.11)}$$

Under the steady-state condition, the rate of useful heat delivered by the module equals the rate of the absorbed energy minus the overall heat loss and converted electricity, expressed as

$$Q_{th} = Q_{abs} - Q_L - Q_e \quad \textbf{(A2.12)}$$

This part of the heat will eventually be converted into the heat received by the water and stored, which is denoted by Q_u. In this case, the module's thermal efficiency can be defined by:

$$\eta_{th} = \frac{Q_{th}}{A_m I} \quad \textbf{(A2.13)}$$

Annex 3

A- The two phase heat transfer coefficient

The two-phase heat transfer Kandiklar correlation [27] has been used and is expressed as follows:

$$\text{For ReLO>100 } h_{TP} = \text{larger of } \begin{cases} h_{TP,NBD} \\ h_{TP,\ CBD} \end{cases} \quad \textbf{(A3.1)}$$

$$h_{TP,NBD} = 0.6683\ Co^{-0.2}(1-x)^{0.8} h_{LO} + 1058.0\ Bo^{0.7}(1-x)^{0.8} F_{Fl} h_{LO} \quad \textbf{(A3.2)}$$

$$h_{TP,NBD} = 1.136\ Co^{-0.9}(1-x)^{0.8} h_{LO} + 667.2\ Bo^{0.7}(1-x)^{0.8} F_{Fl} h_{LO}$$

Where:

$$Co = \left[(1-x)/x\right]^{0.8} \left(\frac{\rho_v}{\rho_L}\right)^{0.5} \quad \textbf{(A3.3)}$$

$$Bo = \frac{q}{G\, h_{fg}}$$

$$\text{For } 10^4 \le Re_{LO} \le 5\ 10^6 h_{LO} = \frac{Re_{LO} Pr_L \left(\frac{f}{2}\right)\left(\frac{k_L}{D}\right)}{1 + 12.7\left(Pr_L^{2/3} - 1\right)(f/2)^{0.5}} \quad \textbf{(A3.4)}$$

$$\text{For } 3000 \le Re_{LO}\ 10^4 h_{LO} = \frac{(Re_{LO} - 1000)\, Pr_L \left(\frac{f}{2}\right)\left(\frac{k_L}{D}\right)}{1 + 12.7\left(Pr_L^{2/3} - 1\right)(f/2)^{0.5}} \quad \textbf{(A3.5)}$$

$$\text{For } 100 \le Re_{LO} \le 1600\ h_{LO} = \frac{Nu_{LO}\, k}{D_h} \quad \textbf{(A3.6)}$$

In the transition region between Reynolds numbers of 1600 and 3000, a linear interpolation is suggested for h_{LO} .

For Reynolds numbers below and equal to 100 ($Re \le 100$), the nucleate boiling mechanism governs, and the following Kandiklar correlation is proposed:

$$\text{For} Re_{LO} \le 100 \quad \textbf{(A3.7)}$$

$$h_{TP} = h_{TP,NBD} = 0.6683 Co^{-0.2}(1-x)^{0.8} h_{LO} + 1058.0 Bo^{0.7}(1-x)^{0.8} F_{Fl} h_{LO} \quad \textbf{(A3.8)}$$

For R-134a the recommended value of F_{Fl} is 1.63.

The vapour quality in the channel port is estimated as:

$$x = \frac{\pi D_h Q_{th}}{\dot{m} h_{fg} \left(N_{ch} N_{hp}\right)} z \quad \textbf{(A3.9)}$$

B- The condensation heat transfer coefficient [28].

For Rev<35000 $h_{cond} = 0.555 \left[\frac{\rho_l g \left(\rho_l - \rho_v\right) k_l^3 h_{fg}}{\mu_l \left(T_{sat} - T_w\right) D}\right]^{1/4}$

For $R_{ev} > 35000$

$$h_{cond} = \frac{k_l}{D} 0.23 \, Re_D^{0.8} Pr_l^{0.4} \left[1 + \frac{2.22}{X_{tt}^{0.89}}\right],$$

$$Re_D = 4 \cdot (1 - x) \dot{/} \left(\pi D \mu_l\right)$$

$$X_{tt} = \left(\frac{1 - x}{x}\right)^{0.9} \left(\frac{\rho_v}{\rho_l}\right)^{0.5} \left(\frac{\mu_l}{\mu_v}\right)^{0.1}$$

C- The fins efficiency in the microchannel [28].

$$\varepsilon_{of} = 1 - N_f A_f \left(1 - \varepsilon_f\right) / A_{tf}; \varepsilon_f = \tanh\left(m_f L_{cf}\right) / m_f L_{cf} \quad \textbf{(A3.9a)}$$

$$m_f = \left(2 \times h_{tp} \times \left(L_e + t_f\right) / \left(K_{hp} L_e t_f\right)\right)^{0.5} \quad \textbf{(A3.10)}$$

$$L_{cf} = b + \frac{\delta_f}{2}; \; A_{tf} = N_f A_f + A_b \; A_b = L_{hp} L_e \; A_f = L_e \delta_f$$

C- Heat transfer in the Annulus [29].

The flow in the annular is characterize by the following Nusselt number and friction factors:

For laminar flow:

Re<2200 $f = 24 \, Re^{-1}$ $Nu = 9.33$ **(A3.11)**

Re>4000 $f = 0.0885 \, Re^{-0.263}$ $Nu = 0.02 \, Re^{0.733} \, Pr^{1/3}$ **(A3.12)**

For $2200 \le Re \le 4000$ an interpolation has been performed.

$$h_w = \frac{Nu \, k_w}{D_{45}} \quad \textbf{(A3.13)}$$

Where D_{45} is the hydraulic diameter based on wetted perimeter, m

$$D_{45} = \frac{\pi \left(D_5^2 - D_4^2\right)}{\pi D_5 + \pi D_4} \quad \textbf{(A3.13a)}$$

Reynolds number Re_w can be calculated by:

$$Re_w = \frac{\rho_{cf} u_l D_{45}}{\mu_{cf}} \quad \textbf{(A3.13b)}$$

The Prandtl number Pr_w is calculated using:

$$Pr_w = \frac{\mu_{cf} c_{pcf}}{k_w} \quad \textbf{(A3.13c)}$$

Where μ_{cf}, c_{pcf}, ρ_{cf}, k_w are the relevant mean dynamic viscosity (kg/m-s), specific heat, density, thermal conductivity of the water.

References

[1] Technology roadmap-solar photovoltaic energy, 2010, International Energy Agency http://www.iea-pvps.org, [accessed 11.04.11].

[2] X. Zhang, X. Zhao, S. Smith and J. Xu, Review of R&D progress and practical application of the solar photovoltaic/thermal (PV/T) technologies, *Renew Sustain Energy Rev* **16** (1), January 2012, 599–617.

[3] H.A. Zondag, Flat-plate PV-Thermal collectors and systems A review, *Renew Sustain Energy Rev* **12**, 2008, 891–959.

[4] C. Lamnatou and D. Chemisana, Photovoltaic/thermal (PVT) systems: a review with emphasis on environmental issues, *Renew Energy* **105**, 2017, 270–287.

[5] T.T. Chow, A review on photovoltaic/thermal hybrid solar technology, *Appl Energy* **87** (2), 2010, 365–379.

[6] Y. Tripanagnostopoulos, M. Souliotis, R. Battisti and A. Corrado, Application aspects of hybrid PV/T solar systems, In: *ISES Solar world congress, Göteborg,* 2003.

[7] Evidence Gathering, Low carbon heating technologies - hybrid solar photovoltaic thermal panels, 2016, Department of Business, Energy, and industrial Strategy, Repoer BRE, Delta-ee.

[8] S. Launay, V. Sartre and J. Bonjour, Parametric analysis of loop heat pipe operation: a literature review, *Int J Therm Sci* **45**, 2007, 621–636, 9. Reay D, Kew P. Heat Pipe (5th edn). Elsevier: Amsterdam, 2006; 48–52, 93–96, 122 and 234–236.10.

[9] M. Bertela and J. Prakash, Transport of thermal energy by a simple two-phase loop, *Int J Energy Res* **12**, 1988, 679–698.

[10] Z. Wang and W. Yang, A review on loop heat pipe for use in solar water heating, *Energy Build* **79**, 2014, 143–154.

[11] J. Zhou, Z. Zhao, X. Ma, Z. Zhu, Z. Qiu, J. Ji and Yu M. Du Z, Experimental investigation of a solar driven direct-expansion heat pump system employing the novel PV/micro-channels-evaporator modules, *Apply Energy* **178**, 2016, 484–495.

[12] Y. Deng, Y. Zhao, Z. Quan and T. Zhua, Experimental study of the thermal performance for the novel flat plate solar water heater with micro heat pipe array absorber, *International conference on solar heating and cooling fo. buildings and industry, SHC 2014, energy procedia* **vol. 70**, 2015, 41–48.

[13] Y. Deng, Y. Zhao, W. Wang, Z. Quan, L. Wang and D. Yu, Experimental investigation of performance for the novel flat plate solar collector with micro-channel heat pipe array (MHPA-FPC), *Appl Therm Eng* **54** (2), 2013, 440–449.

[14] T. Zhu, Y. Diao, Y. Zhao and F. Li, Thermal performance of a new CPC solar air collector with flat micro-heat pipe arrays, *Appl Therm Eng* **98**, 2016, 1201–1213.

[15] G.Q. Li, G. Zhang, W. He, J. Ji, et al., Performance analysis on a solar concentrating thermoelectric generator using the micro-channel heat pipe array, *Energy Convers Manag* **112**, 2016, 191–198.

[16] G.Q. Li, W. Feng, Y. Jin, X. Chen and J. Ji, Discussion on the solar concentrating thermoelectric generation using micro-channel heat pipe array, *Heat Mass Tran* **53** (11), 2017, 3249–3325.

[17] Peyvand Valeh-e-Sheyda, Masoud Rahimi, Ebrahim Karimi and Masomeh Asadi, Application of two-phase flow for cooling of hybrid microchannel PV cells: a comparative study, *Energy Convers Manag* **69**, 2013, 122–130.

[18] M. Kuroda, J. Chang, P. Gwin and R. Mongia, Development of aluminium-water heat pipes, In: *17th International heat pipe conference (17th IHPC) Kanpur, India, October 13-17,* 2013.

[19] Wei He, H. Xiaoqiang, X. Zhao, X. Zhang, J. Shen and J. Ji, Theoretical investigation of the thermal performance of a novel solar loop-heat-pipe facade-based heat pump water heating system, *Energy Build* **77**, 2014, 180–191.

[20] S.A. Kalogirou, Solar energy engineering: process and system, 2009, Elsevier Inc..

[21] H. Imura, H. Kusuda and S. Funatsu, Flooding velocity in a counter-current annular two-phase flow, *Chem Eng Sci* **32**, 1977, pp79–87.

[22] P.K. Swamee and N. Swamee, Discharge equation of a circular sharp-crested orifice, *J Hydraul Res* **48** (1), 2010.

[23] T. Diallo, M. Yu, J. Zhou and X. Zhao, Analytical investigation of the heat transfer limits of a novel solar loop-heat-pipe employing the mini-channel evaporator, *Energies* **11**, 2018, 148, https://doi.org/10.3390/en11010148.

[24] N.H.S. Tay, M. Belusko and F. Bruno, An effectiveness-NTU technique for characterising tube-in-tank phase change thermal energy storage systems, *Appl Energy* **91**, 2012, 309–319.

[25] F.M. White, Fluid mechanics, seventh ed., 2011, McGraw-Hill; New York.

[26] X. Zhang, X. Zhao, J. Xu and X. Yu, Study of the heat transport capacity of a novel gravitational loop heat pipe, *Int J Low Carbon Technol* **8** (3), 2013, 210–223.

[27] S.G. Kandlikar and P. Balasubramanian, An extension of the flow boiling correlation to transition, laminar and deep laminar flows in minichannels and microchannels, *Heat Transfer Eng* **25** (3), 2004, 86–93.

[28] F.P. Incropera, D.P. DeWitt, T.L. Bergman and A.S. Lavine, Fundamentals of heat and mass transfer, seventh ed., 2011, Wiley; Hoboken, NJ.

[29] R. Tiruselvam, W.M. Chin and Vijay R. Raghavan, Double tube heat exchanger with novel enhancement: part II—single phase convective heat transfer, *Heat Mass Tran* **48**, 2012, 1451–1462, https://doi.org/10.1007/s00231-012-0986-x.

[30] S. Wu, Q. Zhang, X. Lan and F. Guo, A heat pipe photovoltaic/thermal (PV/T) hybrid system and its performance Evaluation, *Energy Build* **43**, 2011, 3558–3567.

[31] T. Zhang, G. Pei, Q. Zhu and J. Jie, Experimental study of a novel photovoltaic solar assisted heat pump/loop heat-pipe (PVSAHP/LHP) system, In: *IOP Conf. Series: earth and environmental science* **vol. 52**, 2017, 012017.

[32] X. Zhang, Investigation of a novel solar photovoltaic/loop-heat-pipe heat pump system, Thesis dissertationFebruary 2014, University of Hull.

[33] L. Lu, X. Wang, S. Wang and X. Liu, A new concept of hybrid photovoltaic thermal (PVT) collector with natural circulation, *Heat Mass Tran* **53**, 2017, 2331–2339.

[34] T.T. Chow, J. Ji and W. He, Photovoltaic–thermal collector system for domestic application, *J Sol Energy Eng* **129** (2), 2007, 205–209.

[35] W. He, T.T. Chow, J. Ji, J.P. Lu, G. Pei and L.S. Chan, Hybrid photovoltaic and thermal solar-collector designed for natural circulation of water, *Appl Energy* **83** (3), 2006, 199–210.

[36] J. Ji, J.P. Lu, T.T. Chow, W. He and G. Pei, A sensitivity study of a hybrid photovoltaic/thermal water-heating system with natural circulation, *Appl Energy* **84** (2), 2007, 222–237.

Graphical abstract

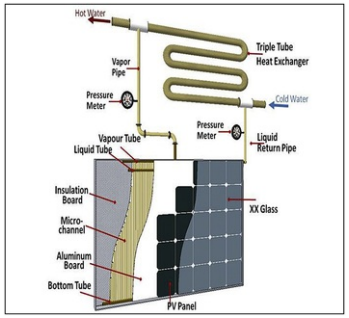

alt-text: Image 1

Highlights

- A novel PVT-LHP system is developed and modelled.

- The PV/LHP system achieves an overall efficiency of 67.8%.
- The system has 28% higher overall efficiency compared to a conventional system.
- The novel PVT-LHP has 2.2 times higher COP compared to a conventional system.

Queries and Answers

Query: Please confirm that the provided email “tdiallo.hull@gmail.com” is the correct address for official communication, else provide an alternate e-mail address to replace the existing one, because private e-mail addresses should not be used in articles as the address for communication.
Answer: please to use my new professionnal address that is: thierno.diallo@cstb.fr

Query: Have we correctly interpreted the following funding source(s) and country names you cited in your article: Innovate UK, United Kingdom; EPSRC, United Kingdom?
Answer: Yes

Query: To maintain sequential order, equations((A2.7a), (A3.9a), (A3.13a), (A3.13b), (A3.13c)) have been renumbered. Please check, and correct if necessary.
Answer: Please replace A2.7a by A2.8 then A2.8 becomes A2.9 and son on until A2.13 thant becomes A2.14. ok for others.

Query: Please confirm that given names and surnames have been identified correctly and are presented in the desired order and please carefully verify the spelling of all authors’ names.
Answer: Yes

Query: Your article is registered as a regular item and is being processed for inclusion in a regular issue of the journal. If this is NOT correct and your article belongs to a Special Issue/Collection please contact s.venkiteswaran@elsevier.com immediately prior to returning your corrections.
Answer: Yes